

科技部補助專題研究計畫成果報告 期末報告

開發以碳六十為核心之兩性自組裝樹枝狀高分子在基因載體上的研究

計畫類別：個別型計畫
計畫編號：MOST 102-2113-M-040-004-
執行期間：102年08月01日至103年10月31日
執行單位：中山醫學大學醫學應用化學系(含碩士班)

計畫主持人：朱智謙

計畫參與人員：碩士班研究生-兼任助理人員：賴鈺森
碩士班研究生-兼任助理人員：歐家禎

處理方式：

1. 公開資訊：本計畫涉及專利或其他智慧財產權，2年後可公開查詢
2. 「本研究」是否已有嚴重損及公共利益之發現：否
3. 「本報告」是否建議提供政府單位施政參考：否

中華民國 104 年 01 月 21 日

中文摘要： 在本研究中，我們成功合成出光敏感兩親性 PAMAM 樹枝狀分子載體。由於結構中具有對 UV 光相當敏感的 ONB 基團，在 365 nm 的光照射之下，會進行光裂解反應使得兩親性分子結構瓦解。我們所設計出來的兩親性分子除了能夠在水中形成自組裝核殼型微胞結構，對於 DNA 分子也具有極佳的結合能力，在低氮磷比例之下會與 DNA 結合形成複合體。更重要的是，相較於一般基因載體的結構降解是透過被動的方式，如 pH 值的改變，我們所設計出來的載體可藉由主動光控的方式，讓結構產生降解而釋放出 DNA。預期可以有效提高細胞基因轉染的效率，後續的生物實驗也正在進行中。

中文關鍵詞： 樹枝狀高分子、基因載體、自組裝微胞、光敏感、光控釋放系統

英文摘要： In summary, we have successfully synthesized the photoresponsive amphiphilic PAMAM dendrons bearing photolabile o-NB building blocks as the DNA carriers. Both amphiphilic dendrons composed of classical and inverse PAMAM dendritic scaffolds reveal similar self-assembly behavior to form the micelle-like pseudodendrimers in aqueous solutions. On the basis of the bipolar functionality, they also demonstrate significant binding affinity with cyclic DNA at low N/P values. Most importantly, thus-formed DNA complexes are readily dissociated under UV light irradiation, because the o-NB group existing in the dendritic structure undergoes efficient photolytic cleavage and thus leads to the effective dendron degradation accompanied by DNA releasing. This study demonstrates the opportunities of using the photoresponsive materials as gene vector to enhance the in vivo transfection efficiency upon exposure to UV light.

英文關鍵詞： Dendrimers, gene vectors, self-assembly micelles, photoresponsive, photo-controlled delivery system

Introduction and motivation

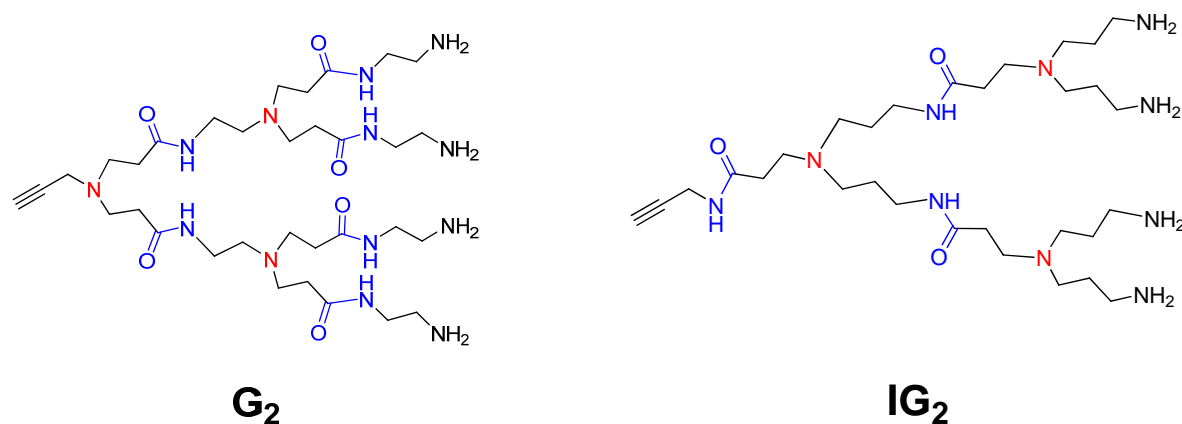
Dendrimers based on the tailor-made surface functional groups and multivalent property have been suggested as promising nanoscale synthetic carriers for the delivery of bioactive materials into target cells. Owing to the tedious and time-consuming processes for preparing the giant dendrimers with well-defined hyperbranched structure, alternatively, using small amphiphilic dendron architectures in which a hydrophobic group at the focal point encourages self-assembly of the resulting amphiphilic dendrons into large “pseudodendrimers”.¹⁻⁴ This supramolecular strategy, allowing the combination of the characteristics of polymers and lipids, can give rise to a synergistic effect particularly in nucleic acids delivery. Recently, several research groups have demonstrated remarkable DNA and small interfering RNA (siRNA) transfection *in vitro* and *in vivo* mediated by these amphiphilic dendrons.⁵⁻⁷

For effective gene delivery, the synthetic carriers must overcome several extra and intracellular barriers including: (1) nucleic acids complexation and protection, (2) cell membrane penetration, (3) endosomal escaping, and (4) nucleic acids releasing for gene expression or knockdown.⁸ Principally, using the “pseudodendrimers” as gene vector takes the advantage of dynamic and responsive association/dissociation towards nucleic acids, which favors not only the encapsulation of nucleic acids through the multivalent ligand array assembled by the dendrons but also rapid disassembly of these complexes under passive triggered condition (i.e., change in pH, ionic strength in target cells). To achieve the controlled release of the nucleic acids after entering the cells, it has been suggested that complete dendron degradation would be required for effective nucleic acids decomplexation. However, the experimental and computer-aid simulation data have reported that structural degradation of the dendrons when bound to nucleic acids becomes ineffective on the transfection time scale even in lower pH associated with endosomes. This key problem associated with barrier 4 on the transfection pathway makes the gene delivery a challenging task particularly for *in vivo* work.

Recently, the concept of phototriggers provide a useful strategy in the photo-controlled drug delivery system (PDDS), because it permits rapid and accurate control over specific site and time with external light stimulation. The biological relevant materials containing a photolabile building block can undergo efficient photolysis through active phototriggers, thus leading to the structural degradation combined with the releasing of biological targets. Among many photolabile groups that have been studied, *o*-nitrobenzyl (*o*-NB) alcohol derivatives have aroused much attention in the field of PDDS.⁹ The *o*-NB alcohol derivatives undergoing an efficient photoisomerization are readily cleaved upon irradiation with UV light (approximately 300-350 nm) and then release a free carboxylic acid and *o*-nitrosobenzaldehyde. Because *o*-NB group is highly sensitive to the exposure of UV light, this photocleavage reaction can be carried out within minutes even in a low-intensity light source. Moreover, simple chemical modifications on aromatic ring allows slight tuning of

absorption profiles of the *o*-NB group. For example, an electron-donating substituent (e.g., OCH₃) functionalized at the para-position of the NO₂ group can bathochromically shift the photocleavage wavelength to the range of 350-400 nm, which is less detrimental to health cells.

In this paper, we aim to develop the amphiphilic dendritic scaffolds with a photolabile building block for creating photoresponsive pseudodendrimer that can achieve controlled release of nucleic acids under active light trigger. Generally, the amphiphilic structure composed of a hydrophilic poly(amido amine) (PAMAM) dendron and a lipophilic cholesterol molecule combines the advantageous gene delivery feature of both lipid and polymer vectors. Moreover, to overcome the barrier 4 described above, the amphiphilic counterpart is further interconnected by a photolabile *o*-NB group, allowing the photo-induced degradation of the amphiphilic structure. Consequently, this strategy provides an active route to accelerate the nucleic acids releasing and to enhance the efficiency gene transfection. Notably, in comparison to classical PAMAM dendrons, novel inverse PAMAM dendrons which have inverse amide bonds are also introduced for the construction the amphiphilic structures (Scheme 1).¹⁰

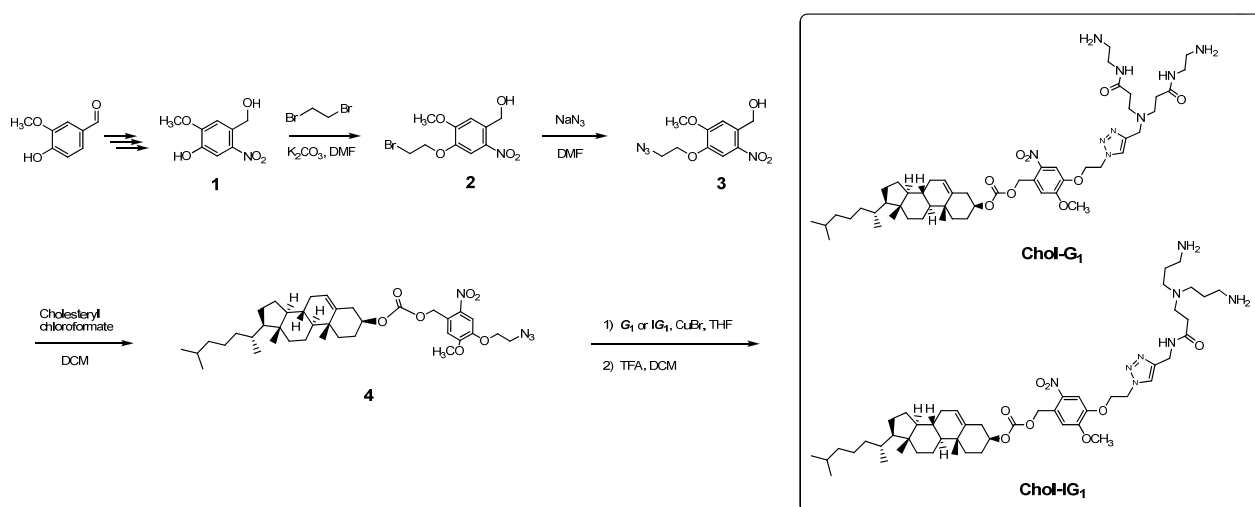


Scheme 1. The structures of classical G₂ and inverse IG₂ PAMAM dendrons.

Results and Discussion

As shown in Scheme 1, classical PAMAM dendrons, namely G_n (n represents the dendron generation and the number of NH_2 groups is equal to 2^n), bearing a propargyl functionality was synthesized via repetitive 1,4-Michael addition and amidation using propargyl amine as starting material. Moreover, the inverse PAMAM dendrons with a COOH focal point, namely IG_n , was prepared by the solid-phase synthetic method developed by Kao's group.¹⁰ Carbodiimide-promoted amidation of IG_n with propargyl amine gives the final propargyl-functionalized inverse dendrons. Herein, all the amino groups of both dendrons were protected by the carbamate (Boc) groups to prevent unwanted complexation of copper catalysts with NH_2 groups during the click reaction.

As shown in Scheme 2, the amphiphilic click adducts were synthesized via [3+2] copper-catalyzed azide-alkyne click reaction (CuAAC).¹¹ Firstly, the *o*-NB alcohol derivative **1** was synthesized from commercial available vanillic aldehyde following a published procedure.¹² A nucleophilic substitution reaction at the phenolic proton yields compound **2**, followed by an azide substitution to give compound **3**. Then a simple esterification of **3** with cholesteryl chloroformate yields the precursor **4**, which allows the "click" conjugation with classical and inverse PAMAM dendrons via conventional CuAAC protocols. Finally, acid-promoted hydrolysis of the click products to remove the Boc protection yields the desired amphiphilic dendrons **Chol- G_n** and **Chol- IG_n** with photolabile *o*-NB building blocks.



Scheme 2. Synthetic route of amphiphilic Chol- G_1 and Chol- IG_1 .

Based on the amphiphilic nature composed of a hydrophilic PAMAM dendron and a lipophilic cholesterol, the **Chol- G_n** and **Chol- IG_n** will assemble into the Percec-type pseudodendrimers in aqueous solution. The structure of the pseudodendrimers are based on a core-shell-like micelle, in which the cholesterol aggregates are sheltered with PAMAM dendrons in water. The hydrophilic and

lipophilic balance (HLB) dominates the size, integrity, and morphology of the micelle-like pseudodendrimers. This self-assembly process was further confirmed by a Nile-red solubilization fluorescence assay, in which hydrophobic Nile-red dyes are used to report on the formation of a hydrophobic domain within an assembled nanostructure.^{3,13} Nile-red is only solubilized when the dendron itself self-assembles into a micelle with a hydrophobic domain. Meanwhile, the fluorescence intensity of Nile-red is dramatically increased. Fig. 1a and 1b show that self-assembly process was observed for **Chol-G₁** and **Chol-IG₁**, with a discontinuity in the fluorescence intensity of Nile-red, plotted against increasing dendron concentration, occurring at the critical aggregation concentration (CAC). The results confirm that the self-assembly process occurs above the CAC. Using this method, the CAC for **Chol-G₁** and **Chol-IG₁** in phosphate buffer solution could be identified as approximately 22 μM , which is comparable to the CAC of cholesterol-based spermine dendrons.¹ In addition, we used dynamic light scattering (DLS) methods assuming a spherical aggregation to further analyze the particle size of the self-assembled aggregates. The dimensions of **Chol-G₁** and **Chol-IG₁** aggregates formed in aqueous buffer solution were approximately 114 ± 0.9 and 130 ± 1.4 nm, respectively.

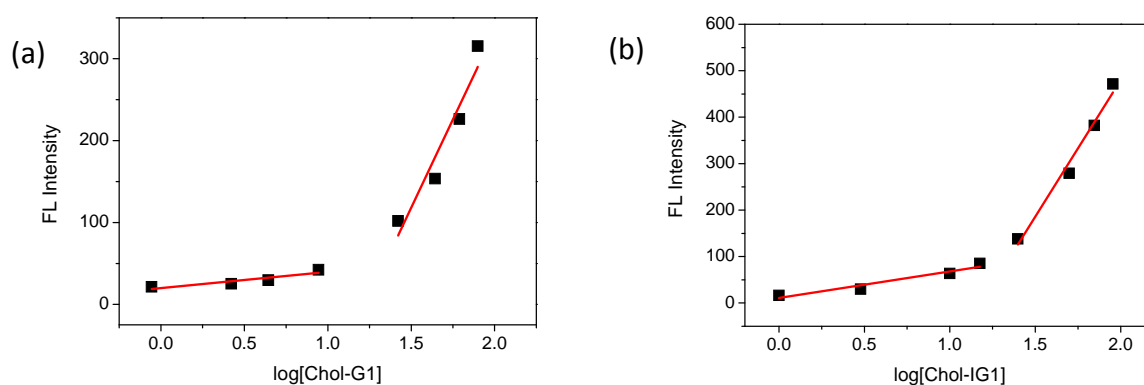


Figure 1. The Nile-red solubilization fluorescence assay of (a) Chol-G₁ and (b) Chol-IG₁.

Because the photocaged *o*-NB derivatives possess moderate absorption in UV region, we then examined the photo-induced degradation of the amphiphilic dendrons by UV-Vis spectroscopic analysis. It is known that the photocleavage reaction can be carried out under UV light, and therefore, both dendron solutions were exposed to 365-nm light-emitting diode (LED) at fixed time intervals (10, 20, and 30 min). Fig. 2a and 2b display apparent change in absorption profiles of **Chol-G₁** and **Chol-IG₁** solutions upon UV light exposure, respectively. The dendron solutions possess red-shifted absorption bands in the UV region (250-400 nm), suggesting the structural decomposition from original *o*-nitrobenzyl carbonate into *o*-nitrosobenzaldehyde after UV light irradiation.¹⁴ Moreover, in both cases, appearance of a detectable absorption peak at 280 nm after light exposure also indicates the formation of *o*-nitrosobenzaldehyde. The UV-Vis analysis confirm that these

amphiphilic dendrons undergo efficient photolysis accompanied with structural degradation.

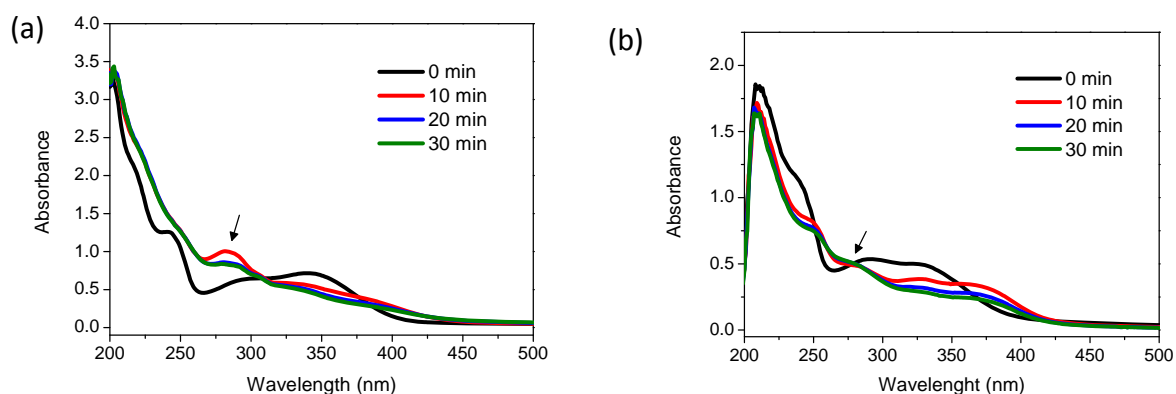


Figure 2. UV-Vis absorption spectra of (a) Chol- G_1 and (b) Chol- IG_1 after 365-nm LED irradiation.

We then carried on to assay the ability of these dendrons to bind pEGFP-C1 reporter DNA (approximate 4700 base pairs) using the standard ethidium bromide (EtBr) displacement fluorescence spectroscopic assay.¹⁵ This method use the competition between the DNA binder and EtBr to access the concentration at which the DNA binder becomes effective. This concentration can be expressed in terms of a charge excess (CE_{50}) value, meaning that the concentration of DNA binder required for half of the EtBr to be displaced from binding to DNA. At such, this value is also equivalent to a minimum nitrogen-to-phosphorus (N/P) ratio that is usually adopted to determine the amount of amine-based binding motifs for effective DNA condensation through electrostatic interactions between the amine and phosphate groups. Initially, EtBr undergoes a large increase in fluorescence intensity upon intercalation with stacks of nucleic acid base pairs. The fluorimetric titration experiments shown in Fig. 3a and 3b reveal the fluorescence quenching of the EtBr/DNA complex in the presence of competing Chol- G_1 and Chol- IG_1 . This is due to a competitive displacement of EtBr by the amine-based dendrons.

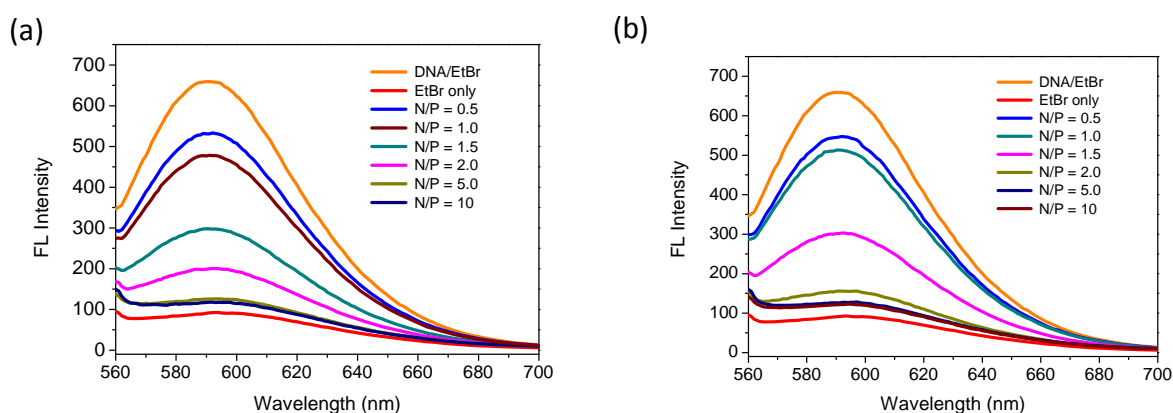


Figure 3. Ethidium bromide (EtBr) displacement fluorescence assay of (a) Chol- G_1 and (b) Chol- IG_1 .

Moreover, kept the DNA and EtBr concentrations constant during all fluorimetric assays, the reduction of fluorescence intensity was found to depend on the administered N/P values. Both amphiphilic dendrons possess significant DNA binding affinity with a calculated CE_{50} value of 1.3, indicating 50% of the EtBr intercalated in the DNA could be successfully replaced by **Chol-G₁** and **Chol-IG₁** at N/P ratio of 1.3 in phosphate buffer solutions. We also performed a control experiment using both **G₁** and **IG₁** dendrons as the DNA binder and found no fluorescent reduction at this N/P value. This result suggests that the amphiphilic structure containing bipolar cholesteryl and PAMAM dendritic counterpart is crucial for DNA complexation. In addition, the DNA complexation was further analyzed by zeta potential measurements. The pristine pEGFP-C1 possesses a negatively surface charge of ca. -54.7 ± 2.6 mV and is neutralized by adding **Chol-G₁** at N/P ratio of 2. The surface potential shifts positively to $+0.47 \pm 0.1$ mV, clearly confirming the effective binding between DNA and the vectors above the CE_{50} .

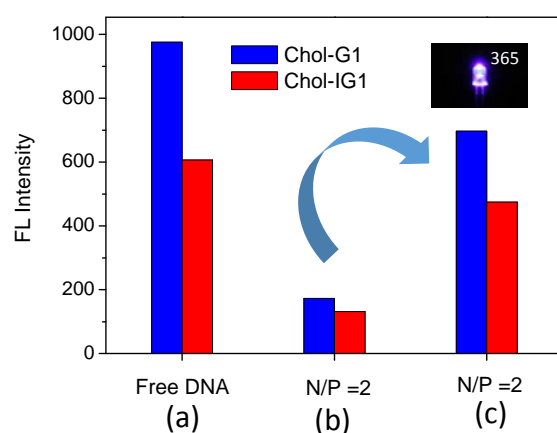


Figure 4. Ethidium bromide (EtBr) displacement fluorescence assay in absence of Chol-G₁ and Chol-IG₁ (a) and in the presence of Chol-G₁ and Chol-IG₁ at N/P = 2 before (b) and after (c) 365-nm LED irradiation.

The EtBr assay can be also used to study the UV-light-induced disassembly of the complexes of DNA and the amphiphilic dendrons. We reasoned that as the dendron degraded under UV-light exposure, the DNA should be released, and the EtBr would reintercalate into the double helix, thus switching its fluorescence back on. Prior to the test, two control experiments confirms: 1) the DNA structure is insensitive to the 365-nm LED, because the fluorescence intensity of EtBr/DNA complex in the absence of amphiphilic dendrons remained at the highest value upon light exposure for 30 min; 2), kept the complex solution in dark for 24 h in the presence of amphiphilic dendrons at N/P ratio of 2, the fluorescence intensity remained essentially at the lowest value. This result suggests that the DNA cannot be released from the electrostatic complexes as the amphiphilic dendrons possess an

intact structure. The bar charts shown in Fig. 4 indicates successful DNA releasing upon UV-light exposure. Firstly, the fluorescence of EtBr at $\lambda_{\text{max}} = 590 \text{ nm}$ was decreased because the EtBr is displaced from the DNA double helix by the presence of **Chol-G₁** and **Chol-IG₁** at N/P ratio of 2. After UV light irradiation within 10 min, the clear increase in fluorescence intensity indicates the serve disassembly of the DNA complexes. On the basis of the UV-Vis analysis, it has been concluded that both **Chol-G₁** and **Chol-IG₁** are highly sensitive to UV light, and therefore, the fluorescence enhancement is apparently due to the EtBr reintercalation into DNA resulting from the photo-induced structural degradation of the amphiphilic dendrons accompanied by DNA releasing. Moreover, the zeta potential of DNA/ **Chol-G₁** complexes drop down from $+0.47 \pm 0.1 \text{ mV}$ before irradiation to $-44.6 \pm 1.5 \text{ mV}$ after irradiation. This negative shift of surface potential also confirms the photo-triggered DNA releasing.

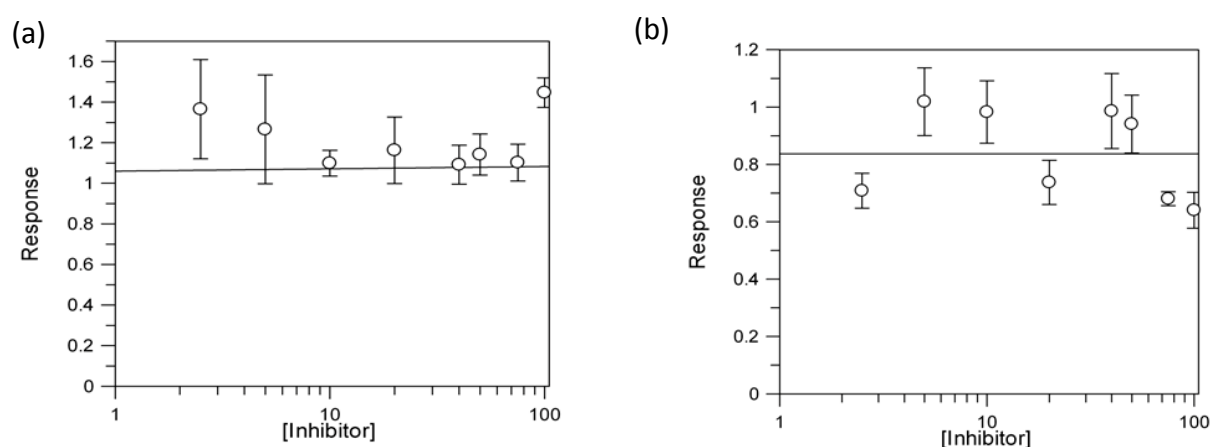


Figure 5. Cytotoxicity tests of (a) Chol-G₁ and (b) Chol-IG₁ for SG cell lines.

Barnard et al. had ever claimed that complete dendron degradation would be necessary for effective DNA release.⁸ When bound to DNA, however, the degradation of the dendrons become ineffective on the transfection-relevant time scale (hours). It is because the DNA complexation may increase the stability of the dendrons against the environmental fluctuation, e.g., the change in pH associated with endosomes. In our case, because of a photolabile *o*-NB building block existing in the dendrons, the structural breakdown even in the presence of DNA can be effectively triggered using UV light irradiation in minutes. This photo-induced strategy allows the DNA releasing on the transfection time scale under an actively triggered route. Moreover, as shown in Fig. 5a and 5b, both **Chol-G₁** and **Chol-IG₁** are nontoxic to the Smulow-Glikcman gingival cell lines (SG cells) up to 100 $\mu\text{g/ml}$. The *in vivo* gene transfection assisted by phototrigger towards SG cells using the photoresponsive amphiphilic dendrons as gene vectors is currently under investigation.

Conclusions

In summary, we have successfully synthesized the photoresponsive amphiphilic PAMAM dendrons bearing photolabile *o*-NB building blocks as the DNA carriers. Both amphiphilic dendrons composed of classical and inverse PAMAM dendritic scaffolds reveal similar self-assembly behavior to form the micelle-like pseudodendrimers in aqueous solutions. On the basis of the bipolar functionality, they also demonstrate significant binding affinity with cyclic DNA at low N/P values. Most importantly, thus-formed DNA complexes are readily dissociated under UV light irradiation, because the *o*-NB group existing in the dendritic structure undergoes efficient photolytic cleavage and thus leads to the effective dendron degradation accompanied by DNA releasing. This study demonstrates the opportunities of using the photoresponsive materials as gene vector to enhance the in vivo transfection efficiency upon exposure to UV light.

Acknowledgments

We would like to thank Chung Shan Medical University and Ministry of Science and Technology (MOST) of Taiwan, for financially supporting this research (NSC102-2113-M-040-004). NMR analysis was performed in the Instrument Center of Chung Shan Medical University, which is supported by Ministry of Education and Chung Shan Medical University.

References

- (1) Posocco, P.; Pricl, S.; Jones, S.; Barnard, A.; Smith, D. K. *Chem. Sci.* **2010**, *1*, 393.
- (2) Jones, S. P.; Gabrielson, N. P.; Wong, C.-H.; Chow, H.-F.; Pack, D. W.; Posocco, P.; Fermeglia, M.; Pricl, S.; Smith, D. K. *Mol. Pharm.* **2011**, *8*, 416.
- (3) Welsh, D. J.; Smith, D. K. *Org. Biomol. Chem.* **2011**, *9*, 4795.
- (4) Barnard, A.; Smith, D. K. *Angew. Chem. Int. Ed.* **2012**, *51*, 6572.
- (5) Kono, K.; Ikeda, R.; Tsukamoto, K.; Yuba, E.; Kojima, C.; Harada, A. *Bioconjugate Chem.* **2012**, *23*, 871.
- (6) Yu, T.; Liu, X.; Bolcato-Bellemin, A.-L.; Wang, Y.; Liu, C.; Erbacher, P.; Qu, F.; Rocchi, P.; Behr, J.-P.; Peng, L. *Angew. Chem. Int. Ed.* **2012**, *51*, 8478.
- (7) Yuba, E.; Nakajima, Y.; Tsukamoto, K.; Iwashita, S.; Kojima, C.; Harada, A.; Kono, K. *J. Controlled Release* **2012**, *160*, 552.
- (8) Barnard, A.; Posocco, P.; Pricl, S.; Calderon, M.; Haag, R.; Hwang, M. E.; Shum, V. W. T.; Pack, D. W.; Smith, D. K. *J. Am. Chem. Soc.* **2011**, *133*, 20288.
- (9) Zhao, H.; Sterner, E. S.; Coughlin, E. B.; Theato, P. *Macromolecules* **2012**, *45*, 1723.
- (10) Huang, A. Y.-T.; Tsai, C.-H.; Chen, H.-Y.; Chen, H.-T.; Lu, C.-Y.; Lin, Y.-T.; Kao, C.-L. *Chem. Commun.* **2013**, *49*, 5784.
- (11) Hung, C.-H.; Chang, W.-W.; Liu, S.-C.; Wu, S.-J.; Chu, C.-C.; Tsai, Y.-J.; Imae, T. *J. Biomed. Mater. Res. A* **2014**, in press.

- (12) Mizuta, H.; Watanabe, S.; Sakurai, Y.; Nishiyama, K.; Furuta, T.; Kobayashi, Y.; Iwamura, M. *Biorg. Med. Chem.* **2002**, *10*, 675.
- (13) Greenspan, P.; Mayer, E. P.; Fowler, S. D. *J. Cell Biol.* **1985**, *100*, 965.
- (14) Corrie, J. E. T.; Barth, A.; Munasinghe, V. R. N.; Trentham, D. R.; Hutter, M. C. *J. Am. Chem. Soc.* **2003**, *125*, 8546.
- (15) Fischer, W.; Quadir, M. A.; Barnard, A.; Smith, D. K.; Haag, R. *Macromol. Biosci.* **2011**, *11*, 1736.

Self-aggregation of amphiphilic [60]fullereryl focal point functionalized PAMAM dendrons into pseudodendrimers: DNA binding involving dendriplex formation

Cheng-Hsiang Hung,¹ Wen-Wei Chang,² Ssu-Ching Liu,² Shang-Jung Wu,¹ Chih-Chien Chu,^{1,3} Ya-Ju Tsai,⁴ Toyoko Imae⁴

¹School of Medical Applied Chemistry, Chung Shan Medical University, Taichung 40201, Taiwan

²School of Biomedical Sciences, Chung Shan Medical University, Taichung 40201, Taiwan

³Department of Medical Education, Chung Shan Medical University Hospital, Taichung 40201, Taiwan

⁴Graduate Institute of Applied Science and Technology, National Taiwan University of Science and Technology, Taipei 10607, Taiwan

Received 8 May 2014; revised 22 July 2014; accepted 23 July 2014

Published online 00 Month 2014 in Wiley Online Library (wileyonlinelibrary.com). DOI: 10.1002/jbm.a.35299

Abstract: In this research, we successfully performed a “click” synthesis of amphiphilic poly(amido amine) dendron-bearing fullereryl conjugate (C₆₀G₁) using a copper(I)-catalyzed azide-alkyne cycloaddition reaction. The strong hydrophobicity of the C₆₀ moiety induces self-assembly of C₆₀G₁ into core-shell-like “pseudodendrimers” with a uniform size distribution and positively charged peripherals. The pseudodendrimers were well-characterized by atomic force microscopy (AFM), transmission electron microscopy, and dynamic light scattering. On the basis of electrostatic interactions, the polycationic C₆₀G₁ assembly can serve as a nonviral gene vector. An ethidium bromide displacement assay and agarose gel electrophoresis both indicated that C₆₀G₁ assembly

forms stable complexes with the cyclic reporter gene (pEGFP-C1) at low nitrogen-to-phosphorous (N/P) ratios. AFM analysis revealed a dynamic complex-formation process, and confirmed the synthesis of C₆₀G₁/pEGFP-C1 hybrids with a particle dimensions less than 200 nm. Fluorescence microscopy and flow cytometry revealed that 51% of HeLa and 43% of MCF-7 cells are positive to the YOYO-1-labeled hybrids at an N/P ratio of 2, being comparable to TurboFect-mediated delivery. © 2014 Wiley Periodicals, Inc. *J Biomed Mater Res Part A*: 00A:000–000, 2014.

Key Words: amphiphilic dendrons, fullerene, gene delivery, PAMAM dendrimer, click chemistry

How to cite this article: Hung C-H, Chang W-W, Liu S-C, Wu S-J, Chu C-C, Tsai Y-J, Imae T. 2014. Self-aggregation of amphiphilic [60]fullereryl focal point functionalized PAMAM dendrons into pseudodendrimers: DNA binding involving dendriplex formation. *J Biomed Mater Res Part A* 2014;00A:000–000.

INTRODUCTION

Poly(amido amine) (PAMAM) dendrimers are considered to be biocompatible, nonimmunogenic drug and gene vehicles because they demonstrate remarkable effectiveness for *in vitro* and *in vivo* medication delivery.^{1–5} However, PAMAM toxicity profiles are problematic for biomedical applications because of the presence of polycationic substituents, and their persistence in cells. Alternatively, using the dendron architectures in which a hydrophobic group at the focal point encourages self-assembly of the resulting amphiphilic dendrons into large “pseudodendrimers.”^{6,7} This supramolecular strategy is a novel concept in the field of dendrimer-mediated nucleic acid delivery.^{8–14} In addition, this type of dendrimers combining the characteristics of cationic polymers and lipids, can give rise to synergistic effects in gene delivery.

Carbon-based nanomaterials, such as fullerenes, nanotubes, and graphene have attracted considerable interest for their biomedical applications, because of their unique *in vitro* and *in vivo* biodistributions and functionalities.^{15–18} In particular, fullerene derivatives that combine 3-dimensionality with defined physicochemical properties are promising candidates for the preparation of bioactive molecules with unique biodistributions.¹⁹ Nakamura and coworkers^{20–23} pioneered stable DNA-C₆₀ hybrids that are capable of effective cell transfection, not only of mammalian cells, but also of pregnant female ICR mice, with distinct organ selectivity; they conducted a systematic structure–activity relationship investigation on a library of 22 cationic fullerene derivatives, and proposed that an appropriate hydrophilic–lipophilic balance (HLB) is essential to synthesize DNA–fullerene complexes for effective gene transfection.

Additional Supporting Information may be found in the online version of this article.

Correspondence to: C.-C. Chu; e-mail: jrchu@csmu.edu.tw

Contract grant sponsor: Chung Shan Medical University and the National Science Council of Taiwan, Republic of China; contract grant number: NSC100-2113-M-040-007-MY2

Although variations in transfection protocol and cell type can dramatically affect transfection efficiency, the size, and morphology of the DNA–vector complexes are also critical parameters to accomplish efficient gene delivery. Pristine C₆₀ is an extremely solvophobic and water-insoluble molecule, and thus the presence of hydrophilic pendant groups confer greater solubility in aqueous media, essential for biological applications.^{24–26} However, the amphiphilic nature of such water-soluble C₆₀ derivatives usually results in spontaneous self-aggregation in aqueous media. Thus, careful manipulation of the amphiphilic counterpart is necessary to achieve a more favorable HLB to form stable gene vehicles with appropriate shape and morphology (e.g., spheroid or vesicle-like), thus facilitating DNA complexation, cellular uptake, and gene transfection.^{27–30}

In the current study, we demonstrate a facile synthesis of amphiphilic PAMAM dendron-bearing fullerene derivative, by using an efficient Cu(I)-catalyzed azide-alkyne cycloaddition (CuAAC).³¹ We found that the click cluster, interconnecting the diazido-functionalized fullerene and PAMAM dendrons bearing a propargyl focal point via a 1,4-triazole linkage, is highly water-soluble and is readily prepared in high yield without the need for chromatographic purification. Amphiphilic dendrons containing an extremely hydrophobic fullerene moiety and a hydrophilic PAMAM dendritic scaffold, favor the formation of nanoparticles with a uniform size distribution in water. Atomic force microscopy (AFM) analysis revealed that these particles could condense plasmid DNA into stable complexes with desirable dimensions, at low nitrogen-to-phosphorus (N/P) ratios. Moreover, the fullerodendron assembly also exhibited remarkable gene delivery efficiency toward the target cell lines.

EXPERIMENT

Materials and instruments

Pure C₆₀ was purchased from Uni-onward Corporation and used as received. Other chemicals used for organic synthesis were obtained as high-purity reagent-grade chemicals from either Acros or Sigma-Aldrich and used without further purification. Organic solvents were AR grade and purchased from either Mallinckrodt or Echo chemicals. Ethylenediamine (EDA) and dichloromethane (DCM) were dried over calcium hydride under N₂ before used. Tetrahydrofuran (THF) and toluene were distilled over sodium under N₂ in the presence of benzophenone as the indicator prior to use.

Gel permeation chromatography (GPC) was conducted at 35°C using a Shodex Sugar KS-802 column on an assembled instrument that was equipped with pump (Water Model-501), column oven, and refractive index detector (Schambeck SFD GmbH, RI-2000) connected in series. ¹H (400 MHz)- and ¹³C (100 MHz)-NMR spectra were recorded on a Varian Mercury Plus 400 MHz spectrometer at room temperature using CDCl₃, DMSO-*d*₆, or D₂O as the solvent. Spectral processing (Fourier transform, peak assignment and integration) was performed using MestReNova 6.2.1 software. Matrix-assisted laser desorption ionization/time-of-flight mass spectrometry (MALDI-TOF-MS) was performed on a Bruker AutoFlex III TOF/TOF system in positive ion

mode using either 2,5-dihydroxybenzoic acid or α-cyano-4-hydroxycinnamic acid as the desorption matrix. Fourier-transform infrared (FT-IR) and ultraviolet–visible (UV-Vis) absorption spectra were performed on a Bruker Alpha FT spectrometer and on a Thermo Genesys 10S UV-Vis spectrometer, respectively. Fluorescence spectroscopic analysis was carried out either on a Hitachi F-2500 spectrometer or on a Molecular Devices FlexStation 3 microplate reader at 25°C.

Synthesis of PAMAM dendron G₁

A methanol solution (370 mL) of propargylamine (6.01 g, 0.109 mol) was added slowly into a methanol solution (110 mL) of methyl acrylate (28.1 g, 0.326 mol) under 0°C. The reaction mixture was allowed to warm to room temperature and stirred for 3 days. The volatiles were removed under reduced pressure using a rotary evaporation to give half-generation dendron quantitatively. Then this compound (6.25 g, 27.5 mmol) dissolved in dry methanol (90 mL) was added dropwise into a methanol solution (370 mL) of EDA (66.1 g, 1.1 mol) under 0°C over a period of 30 min. The reaction mixture was allowed to warm to room temperature and stirred for 3 days under a N₂ balloon until complete disappearance of terminal methyl ester groups. The solvent was removed under reduced pressure using a rotary evaporation, and excess EDA was carefully removed by azeotropic distillation at 35°C using toluene and methanol mixture (9:1) to afford product G₁ as a yellowish gum (30.0 g, 97%). ¹H-NMR (400 MHz, CDCl₃): δ = 2.22 (t, *J* = 2.3 Hz, 1H), 2.38 (t, *J* = 5.8 Hz, 4H), 2.81–2.86 (m, 8H), 3.29 (dd, *J* = 11.6, 5.8 Hz, 4H), and 3.43 (d, *J* = 2.3 Hz, 2H).

Synthesis of PAMAM dendron G₂

A methanol solution (40 mL) of G₁ (3.44 g, 12.1 mmol) was added slowly into a methanol solution (25 mL) of methyl acrylate (6.27 g, 72.8 mmol) under 0°C. The reaction mixture was allowed to warm to room temperature and stirred for 3 days. The volatiles were removed under reduced pressure using a rotary evaporation to give half-generation dendron quantitatively. This compound (6.39 g, 10.2 mmol) dissolved in dry methanol (35 mL) was added dropwise to a methanol solution (270 mL) of EDA (48.9 g, 0.814 mol) under 0°C over a period of 30 min. The reaction mixture was allowed to warm to room temperature and stirred for 3 days under a N₂ balloon until complete disappearance of terminal methyl ester groups. The solvent was removed under reduced pressure using a rotary evaporation, and excess EDA was carefully removed by azeotropic distillation at 35°C using toluene and methanol mixture (9:1) to afford product G₂ as a yellowish gum (8.15 g, 91%). ¹H-NMR (400 MHz, CDCl₃): δ = 2.22 (t, *J* = 2.3 Hz, 1H), 2.31–2.38 (m, 12H), 2.52 (t, *J* = 6.0 Hz, 4H), 2.74 (t, *J* = 6.0 Hz, 8H), 2.81 (t, *J* = 6.0 Hz, 12H), 3.22–3.31 (m, 12H), and 3.44 (d, *J* = 2.3 Hz, 2H). MALDI-TOF-MS: Calcd. For (M + H)⁺ C₃₃H₆₆N₁₃O₆: 740.5; found: 740.6.

Boc-protection of PAMAM dendron G₁

A methanol solution (10 mL) of G₁ (1.08 g, 3.81 mmol) was added slowly into a methanol solution (10 mL) of di-tert-

butyl pyrocarbonate (2.50 g, 11.4 mmol) under -10°C . The solution was stirred for 30 min and then allowed to warm to room temperature. After stirred for 4 h, the mixture was extracted with DCM (50 mL \times 3); the combined organic phase was washed with brine (20 mL \times 2) and dried over magnesium sulfate. After rotatory evaporation to dryness, repetitive precipitation in hexane afforded Boc-protected G_1 ($\text{G}_1\text{-Boc}$) as a yellowish solid (1.75 g, 95%). $^1\text{H-NMR}$ (400 MHz, CDCl_3): $\delta = 1.44$ (s, 18H), 2.22 (t, $J = 2.3$ Hz, 1H), 2.36 (t, $J = 5.9$ Hz, 4H), 2.82 (t, $J = 5.9$ Hz, 4H), 3.23–3.27 (m, 4H), 3.33–3.37 (m, 4H), 3.41 (d, $J = 2.3$ Hz, 2H), and 5.41 (s, 2H).

Synthesis of (4-(azidomethyl)phenyl)methanol 1

A dry DCM solution (20 mL) of thionyl chloride (6.55 g, 55.1 mmol) in a dropping funnel was added dropwise into a dry DCM solution (40 mL) of *p*-xylylene glycol (6.90 g, 49.9 mmol) at 0°C under nitrogen. The mixture was stirred at 0°C for 1 h and then continued stirring under room temperature for an additional 20 h. The volatiles were removed under reduced pressure, and the residue was then extracted by DCM (50 mL \times 3). After rotatory evaporation to dryness, further purification was carried out by flash column chromatography (SiO_2 , ethyl acetate/hexane 2:3) to give (4-(chloromethyl)phenyl)methanol (5.15 g, 66%) as a colorless liquid. This compound (4.86 g, 31.0 mmol) dissolved in dry *N,N*-dimethylformamide (DMF, 60 mL) was then added dropwise into a DMF suspension of sodium azide (20.3 g, 0.310 mol) under nitrogen. The mixture was then stirred at 80°C overnight. The organic solvent was removed under reduced pressure, and the residue was then extracted by ethyl acetate (50 mL \times 2), followed by rotatory evaporation to give **1** as a colorless liquid (3.80 g, 75%). $^1\text{H-NMR}$ (400 MHz, CDCl_3): $\delta = 2.60$ (s, 1H), 4.30 (s, 2H), 4.62 (s, 2H), 7.29 (d, $J = 8.1$ Hz, 2H), and 7.33 (d, $J = 8.1$ Hz, 2H).

Synthesis of bis(4-(azidomethyl)benzyl) malonate 2

A dry DCM solution of dicyclohexylcarbodiimide (DCC, 6.95 g, 33.7 mmol) was added dropwise into a mixed dry DCM/THF (30:10 mL) solution of **1** (5.5 g, 33.7 mol), malonic acid (1.59 g, 15.3 mmol), and 1-hydroxybenzotriazole (HOBT, 695 mg, 10 wt % of DCC) under nitrogen at 0°C . After 30 min, the mixture was then stirred under room temperature overnight. The reaction mixture was cooled to 0°C to insure complete precipitation of the byproduct dicyclohexylurea, which is then quickly removed by vacuum filtration. After rotatory evaporation to dryness, further purification was carried out by flash column chromatography (SiO_2 , ethyl acetate/hexane 2:3) to give **2** as a colorless liquid (3.50 g, 58%). $^1\text{H-NMR}$ (400 MHz, CDCl_3): $\delta = 3.49$ (s, 2H), 4.34 (s, 4H), 5.18 (s, 4H), 7.31 (d, $J = 8.2$ Hz, 4H), and 7.34 (d, $J = 8.2$ Hz, 4H).

Synthesis of bis-azido-fullerene derivative 3

A dry toluene (350 mL) solution of C_{60} (350 mg, 0.486 mmol) was added with I_2 (148 mg, 0.583 mmol), **2** (201.3 mg, 0.510 mmol), and 1,8-diazabicycloundec-7-ene (DBU, 155 mg, 1.02 mmol) sequentially. The mixture was

stirred under room temperature for 24 h. After rotatory evaporation to dryness, further purification was carried out by flash column chromatography (SiO_2 , DCM/hexane 7:3) to give **3** as a brown solid (270 mg, 50%). $^1\text{H-NMR}$ (400 MHz, CDCl_3): $\delta = 4.36$ (s, 4H), 5.48 (s, 4H), 7.34 (d, $J = 8.4$ Hz, 4H), and 7.44 (d, $J = 8.4$ Hz, 4H).

Synthesis of C_{60}G_1 click cluster

A dry THF solution (30 mL) of $\text{G}_1\text{-Boc}$ (246 mg, 0.509 mmol), **3** (270 mg, 0.242 mmol), and CuBr (73.2 mg, 0.510 mmol) was vigorously stirred under room temperature for 3 days and then quenched with aqueous ammonia. The organic solvent was removed using rotatory evaporation, and the residue was then extracted by ethyl acetate (50 mL \times 2) to give Boc-protected C_{60}G_1 as a dark brown solid. Carbamate deprotection is readily carried out by acid-promoted hydrolysis. Trifluoroacetic acid (TFA, 611 mg, 5.36 mmol) was added dropwise into a dry DCM solution (15 mL) of Boc-protected C_{60}G_1 (226 mg, 0.109 mmol). The mixture was then stirred under room temperature for 2 days, and the volatiles were removed under reduced pressure. The mixture was washed with hexane repetitively to remove excess acid, and then freeze-drying afforded C_{60}G_1 as a brown fluffy powder (207 mg, 89%). $^1\text{H-NMR}$ (400 MHz, CDCl_3): $\delta = 2.82$ (t, $J = 6.4$ Hz, 8H), 3.09 (t, $J = 6.4$ Hz, 8H), 3.47 (t, $J = 6.4$ Hz, 8H), 3.56 (t, $J = 6.4$ Hz, 8H), 4.14 (d, $J = 2.0$ Hz, 4H), and 7.87 (s, 2H). MALDI-TOF-MS: Calcd. For $(\text{M} + \text{H})^+$ $\text{C}_{105}\text{H}_{66}\text{N}_{16}\text{O}_8$: 1679.75; found: 1680.46. Calcd. For $(\text{M} + \text{Na})^+$ $\text{C}_{105}\text{H}_{66}\text{N}_{16}\text{NaO}_8$: 1702.74; found: 1702.53.

Ethidium bromide displacement assay

0.5 mL of pEGFP-C1 solution ($1 \mu\text{g mL}^{-1}$) and 7 μL of ethidium bromide (EtBr) solution (0.1 mg mL^{-1}) were mixed thoroughly in vials, followed by adding 8 μL of C_{60}G_1 solutions to achieve the desired N/P = 0.6, 0.8, 1.0, 1.2, and 2.0. Aliquots (200 μL) of thus-prepared solutions were then added into each well of 96-well black plates for the fluorescence measurement. 7 μL of EtBr (0.1 mg mL^{-1}) in ultrapure water (508 μL) was measured as the background fluorescence of EtBr, and the solution that only contains pEGFP-C1 and EtBr in 1:1 binding ratio corresponds to the N/P = 0 with maximum emission intensity. The fluorescence measurement was performed on Molecular Devices FlexStation 3 microplate reader using an excitation wavelength of 260 nm, and the emission spectra were recorded from 540 nm to 700 nm.

Characterization of complex morphology, size, and ζ -potential

For atomic force microscopic analysis, 5 μL of each sample was placed on a freshly cleaved mica sheet. After 5 min incubation at room temperature, the sheet was washed twice with 100 μL of double-distilled H_2O . The prepared samples were first dried from the edge of the mica sheet using a paper tissue, then by exposure to gentle air flow for 10 min. The samples were then immediately subjected to AFM study. We used a Nanoscope IIIa Multimode scanning probe microscope from Digital Instruments (Veeco Metrology Group,

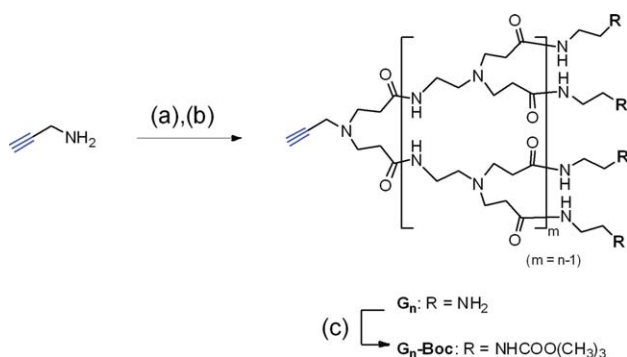


FIGURE 1. Synthesis of G_1 and G_2 PAMAM dendrons bearing a propargyl focal point. (a) methyl acrylate, methanol; (b) EDA, methanol; and (c) di-tert-butyl pyrocarbonate, methanol. [Color figure can be viewed in the online issue, which is available at wileyonlinelibrary.com.]

Santa Barbara, CA) in contacting mode with scan rate of 2.441 Hz and tip velocity of $2.35 \mu\text{m s}^{-1}$. Analyses of the images were carried out using the Nanoscope III software version 5.31R1. Dynamic light scattering (DLS) and ζ -potential measurements were performed on Malvern Zetasizer Nano series. Transmission electron microscopy (TEM) images were taken by a Hitachi H-7000 electron microscope with Hamamatsu C4742-95 digital camera operated at an accelerating voltage of 100 kV.

Cellular uptake of the $C_{60}G_1$ /DNA complexes

HeLa cells and MCF-7 cells were obtained from the American Type Culture Collection (ATCC, Manassas, VA). MCF-7 cells were cultured in MEM α medium (Life Technologies Corporation) supplemented with 10% fetal bovine serum (Hyclone), bovine insulin ($5 \mu\text{g mL}^{-1}$, Sigma-Aldrich), sodium pyruvate (1 mM; Biological Industries), antibiotics (100 U mL^{-1} penicillin and $100 \mu\text{g mL}^{-1}$ streptomycin; Life Technologies Corporation), and Glutamax (2 mM; Life Technologies Corporation). HeLa cells were cultured in DMEM medium (Life Technologies Corporation) with supplements as used for MCF-7 cultivation except for bovine insulin. The cells were maintained in a 5% CO_2 air humidified atmosphere at 37°C .

To evaluate the cellular uptake efficiency of the $C_{60}G_1$ /DNA complex, pEGFP-C1 (Clontech) was labeled with YOYO-1 fluorescent dye (Life Technologies Corporation). Briefly, 500 μL of pEGFP-C1 solution in water ($1 \mu\text{g mL}^{-1}$) was mixed with 4 μL of 200 μM YOYO-1 and incubated at room temperature for 10 min. Then, 3.2 μL of $C_{60}G_1$ ($0.5 \mu\text{g mL}^{-1}$) and TurboFect (Fermentas, Thermo Scientific, Pittsburgh, PA) containing YOYO-1-labeled plasmid DNA were added to the cells with the complete medium (DMEM with 10% FBS and antibiotics), and further cultured for 2 h before being harvested for fluorescence microscope and flow cytometric analysis.

Fluorescence microscopy and flow cytometry

For observation of GFP+ cells, cells were observed for green fluorescence signals with inverted fluorescent microscopy (Axioskop 2, ZEISS, Germany) with 100 W halogen lamp, 480/30 nm band-pass blue excitation filter, a 505 nm dichroic mirror, and a 535/40 nm band-pass barrier filter. Images were

captured with cool CCD camera and processed with MetaMorph Software (Molecular Devices). For quantification with GFP+ cells, cells were harvested with trypsin/EDTA, resuspended in 200 μL of PBS/1% bovine serum albumin (Sigma-Aldrich), and analyzed by flow cytometry (Epics XL, Beckman Coulter). The green fluorescence emission (525 nm) illuminated with 488 nm blue laser and signals were collected with software provided by the manufacturer. The percentage and mean fluorescence intensity of GFP+ cells were further analyzed by WinMDI software (The Scripps Research Institute, San Diego). Each data shown in Figure 9 was expressed as mean \pm standard deviation of three experiments.

Agarose gel electrophoresis analysis of complexing capacity between $C_{60}G_1$ and DNA

0.5 μg of pEGFP-C1 plasmid DNA was dissolved in nuclease-free H_2O and $C_{60}G_1$ was then added at different N/P ratio (range from 0.5 to 2.0) to final volume of 15 μL . After mixing well and incubating at room temperature for 30 min, the $C_{60}G_1$ /DNA solutions were added with 3 μL of Novel juice DNA loading dye (GeneDirex), loaded into wells of 1.0% agarose gel, and performed electrophoresis in TAE buffer (40 mM Tris-acetate, 1 mM $\text{Na}_2\text{-EDTA}$, pH = 8.5) at 150 V for 1 h. DNA signals were detected by SafeBlue Imager System (Major Science, Saratoga, CA) with a blue light LED source to visualize the DNA bands and images were captured by a digital camera (Canon G15; Ohta-ku, Tokyo, Japan). The intensities of DNA bands were analyzed by ImageJ software (NIH, Bethesda, MA).

RESULTS AND DISCUSSION

Material synthesis and characterization

Our strategy for the synthesis of amphiphilic C_{60} -PAMAM-dendron click clusters comprised 2 parts. (1) The preparation of a counterpart: the NH_2 -terminated PAMAM dendron

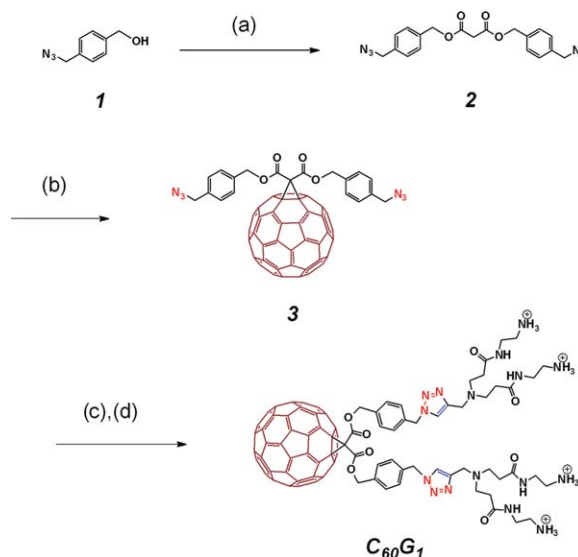


FIGURE 2. Synthesis of amphiphilic PAMAM dendron-bearing C_{60} click cluster ($C_{60}G_1$). (a) malonic acid, DCC, HOBT, THF/ CH_2Cl_2 , 0°C to room temperature; (b) C_{60} , DBU, I_2 , toluene; (c) $G_1\text{-Boc}$, CuBr, THF; and (d) TFA, CH_2Cl_2 . [Color figure can be viewed in the online issue, which is available at wileyonlinelibrary.com.]

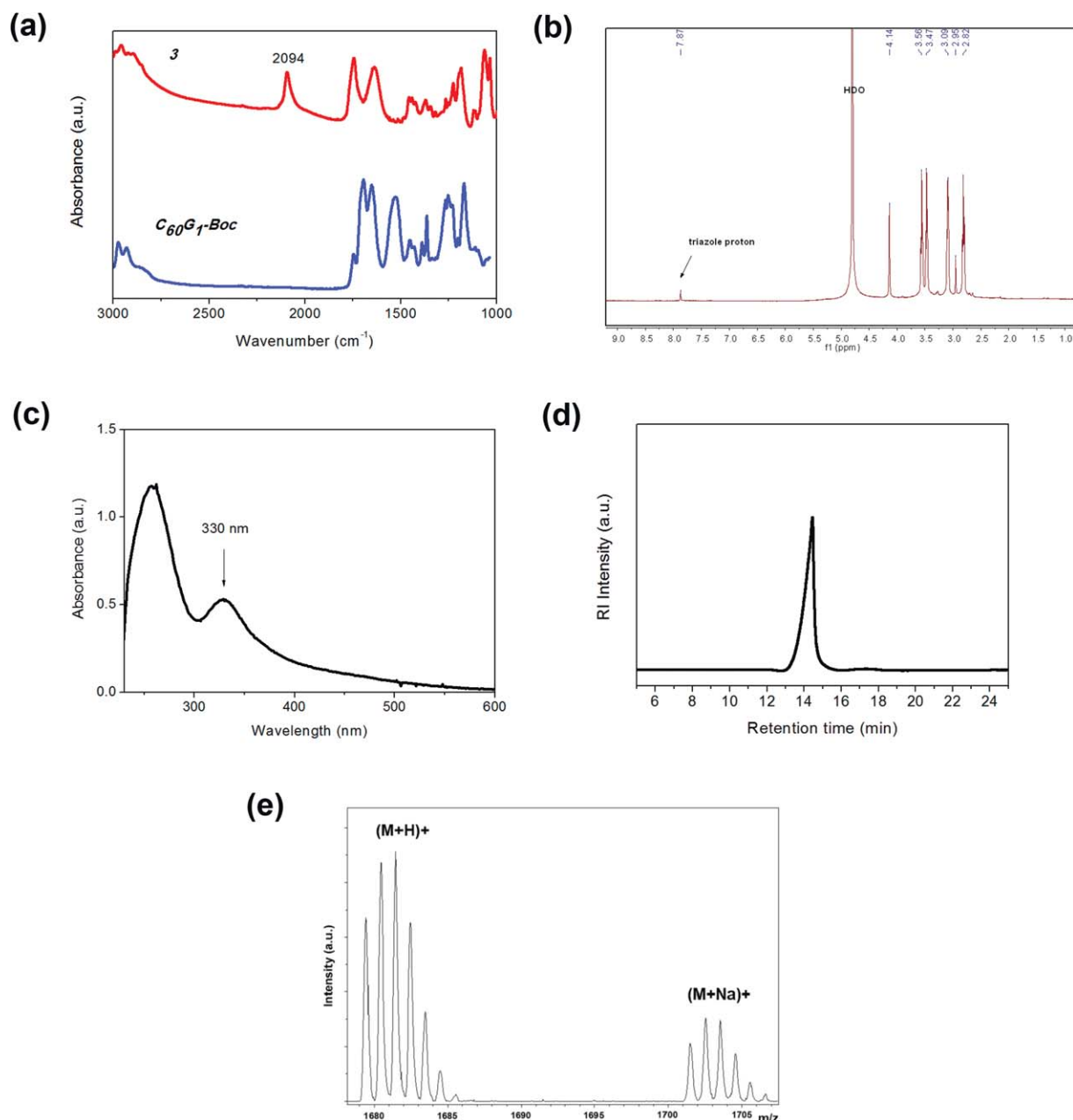


FIGURE 3. (a) FT-IR spectra of **3** and Boc-protected $C_{60}G_1$. (b) 1H -NMR spectrum, (c) UV-Vis spectrum, (d) GPC chromatogram, and (e) MALDI-TOF-MS spectrum of $C_{60}G_1$. [Color figure can be viewed in the online issue, which is available at wileyonlinelibrary.com.]

was prepared by a divergent pathway using propargylamine as the focal point. As shown in Figure 1, a conventional 2-step procedure consisting of a Michael addition followed by amidation produces the G_1 PAMAM dendron. All NH_2 terminals were then protected with Boc groups to prevent unwanted complexation with the copper catalysts; (2) as shown in Figure 2, the diazido-functionalized fullerene derivative was prepared in high yield by a Bingel reaction. The conjugation of the as-prepared PAMAM dendrons and the C_{60} derivative was conducted through a CuAAC ("click" reaction) to produce the protected click clusters. Finally, acidic hydrolysis was performed to deprotect the amino

groups, and produce the highly water-soluble amphiphilic C_{60} and G_1 PAMAM dendron conjugate, namely $C_{60}G_1$.

$C_{60}G_1$ and its precursors were fully characterized by 1H -NMR, FT-IR, UV-Vis spectroscopy, GPC, and MALDI-TOF mass spectrometry. The 1H - and ^{13}C -NMR spectra of compounds **2** and **3** (Supporting Information Figs. S1 and S2) clearly indicate the successful synthesis of a Bingel adduct with diazido groups, by the disappearance of the malonate center protons at 3.5 ppm. Notably, although the azido group could attack the fullerene moiety to cause cycloaddition, compound **2** was stable in dilute solution. FT-IR spectroscopy confirmed the success of the click coupling

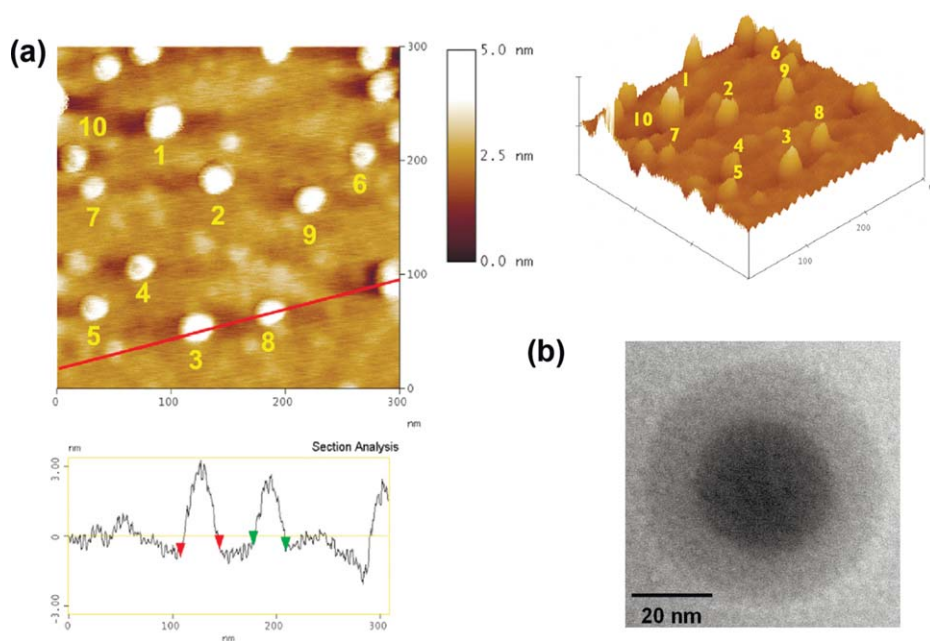


FIGURE 4. (a) Atomic force micrograph and section analysis for $C_{60}G_1$ aggregates on mica surface. The particle dimension averaged by 10 selected particles is 22.4 ± 3.7 nm. (b) Transmission electron micrograph of core-shell-like $C_{60}G_1$ aggregates. [Color figure can be viewed in the online issue, which is available at wileyonlinelibrary.com.]

between the Boc-protected G_1 PAMAM dendron and the diazido fullerene, by the disappearance of the azide stretching band at 2094 cm^{-1} [Fig. 3(a)], and by the appearance of characteristic proton and carbon resonances of the click counterpart in the $^1\text{H-NMR}$ spectra (Supporting Information Fig. S3). Finally, complete deprotection of the Boc groups was confirmed by the disappearance of the corresponding protons at 1.5 ppm from the $^1\text{H-NMR}$ spectrum, supporting the formation of the highly water-soluble cationic C_{60} derivative bearing two NH_2 -terminated G_1 PAMAM dendrons [Fig. 3(b)]. Additionally, the appearance of the triazole proton resonance at 7.9 ppm suggests that CuAAC click coupling was successful, indicating the exclusive formation of the 1,4-regioisomer.³² Moreover, UV-Vis analysis of the as-prepared click clusters [Fig. 3(c)] show a broad absorption maximum at approximately 330 nm, clearly indicating the existence of a fullerene core. Aqueous phase GPC combined with cationic exchange chromatography [Fig. 3(d)] revealed monodispersed elution peaks for $C_{60}G_1$, confirming that the click reaction produced a single product in high purity. MALDI-TOF mass spectrometry results support our proposed structure by demonstrating an exact match between calculated and observed molar masses for the $C_{60}G_1$ click cluster [Fig. 3(e)].

Self-aggregation of amphiphilic $C_{60}G_1$ and DNA complexes

Because of its amphiphilic nature, $C_{60}G_1$ assembles into core-shell-like micelles rather than remaining in a single molecular form in aqueous media.³³ Therefore, we used AFM to analyze the $C_{60}G_1$ self-aggregation behavior. Figure 4(a) shows microscopic images of $C_{60}G_1$ deposited on a

freshly cleaved mica surface, clearly confirming the formation of nanoclusters, with an average dimension of 22.4 ± 3.7 nm. The results of DLS experiments were in agreement with the AFM results, indicating comparable dimensions for these micelle-like nanoparticles, with a z-average size distribution of 24.8 ± 0.2 nm, and a polydispersity index of 0.255 ± 0.008 . Both sets of data are consistent with the magnitude of primary micelles comprising a hydrophobic C_{60} core and hydrophilic PAMAM dendron shell. Moreover, TEM analysis demonstrated a micelle-like structure with sharp contrast between the core and shell components [Fig. 4(b)].

Recently, López et al.³⁴ reported a series of regioisomeric dendron-fulleropyrrolidines with no aggregation occurring up to $10^{-3}\text{ mol L}^{-1}$. However, on the basis of AFM and DLS analysis, we found that the $C_{60}G_1$ favors the formation of nanoparticles at much lower concentration of approximately $5 \times 10^{-6}\text{ mol L}^{-1}$. Thus, C_{60} could serve as a hydrophobic building block, and so drive PAMAM dendron assembly to form a “pseudodendrimer.” Moreover, zeta-potential measurement further indicated that these C_{60} -centered pseudodendrimers carry multiple positive charges on their surfaces (22.3 ± 5.2 mV), allowing electrostatic interactions with polyanionic targets such as plasmid DNA.

We evaluated the binding affinity of amphiphilic $C_{60}G_1$ toward pEGFP-C1 (4731 base pairs) using an EtBr displacement assay.³⁵ The DNA intercalating agent EtBr is commonly used in molecular biology to detect nucleic acids. The competition for binding with DNA, between EtBr reagents and polyamine-based vectors toward DNA, allows us to determine the minimum N/P ratio necessary for effective complexation. In the assay, the optimized N/P ratio is

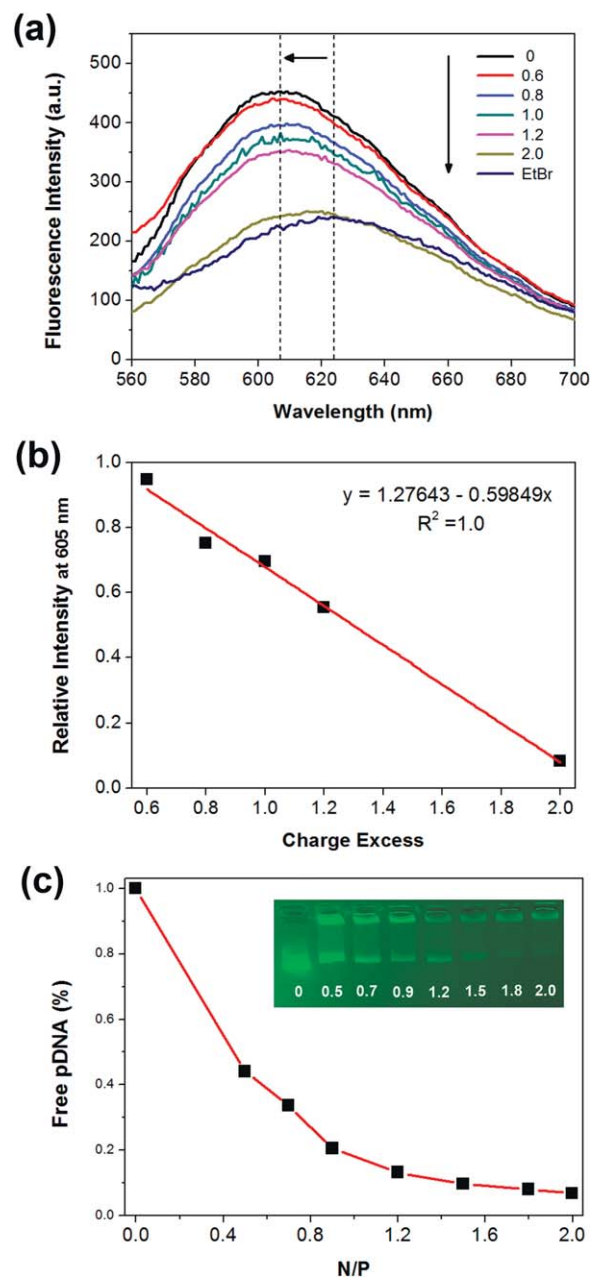


FIGURE 5. (a) Fluorescence titration data for the addition of $C_{60}G_1$ to DNA at various nitrogen-to-phosphorous (N/P) ratios. The maximum fluorescence intensity corresponds to the 1:1 binding of EtBr and a DNA base in the absence of $C_{60}G_1$, and the minimum intensity corresponds to the amount of free EtBr in water. (b) The linear correlation of relative fluorescence intensities at 605 nm versus the charge excess values. (c) Agarose gel electrophoresis analysis for determining the optimized binding capacity of $C_{60}G_1$ at various N/P ratios. [Color figure can be viewed in the online issue, which is available at wileyonlinelibrary.com.]

expressed as a 50% charge excess (CE_{50}) value, which represents the “excess charge” on the cationic vector relative to anionic DNA that is required for 50% EtBr displacement. A lower CE_{50} value, provided by a smaller N/P ratio, represents more effective binding of the 2 components. Figure 5(a) provides fluorescence titration data for the addition of $C_{60}G_1$, where the maximum fluorescence intensity corre-

sponds to the 1:1 binding of EtBr and a DNA base in the absence of $C_{60}G_1$, and the minimum intensity corresponds to the amount of free EtBr in water. We attributed the enhanced and blue-shifted emission pattern arising from the intercalating complex to the less polar environment inside the DNA helix. Emission intensity continually decreased with increasing $C_{60}G_1$ concentration, suggesting that intercalating EtBr molecules were gradually displaced by C_{60} -based

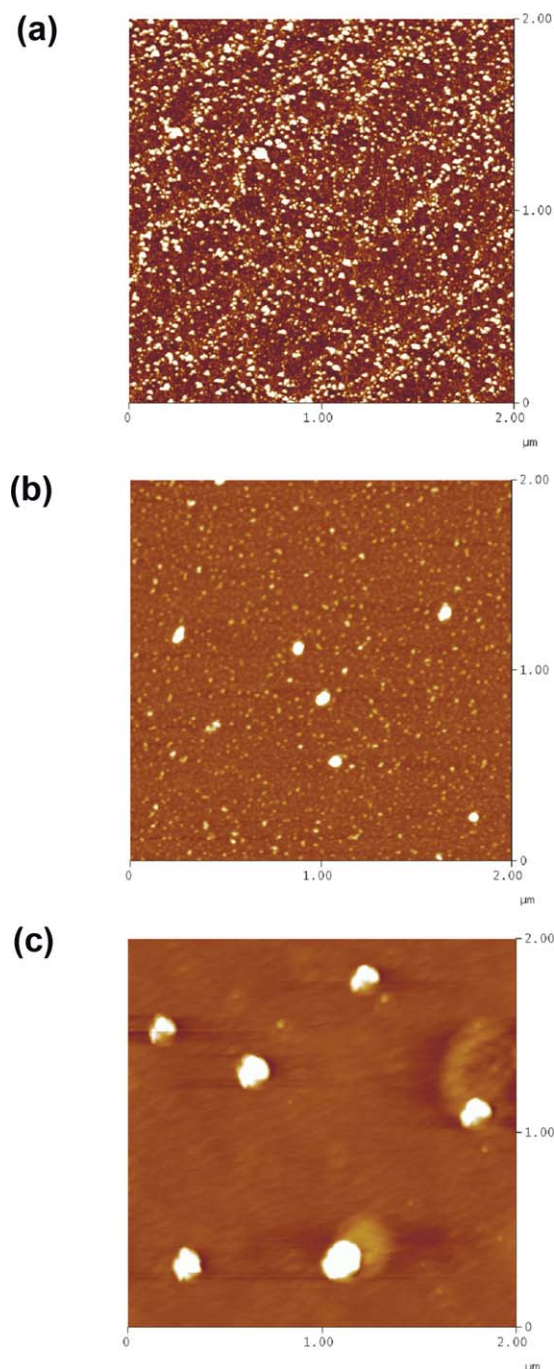


FIGURE 6. Atomic force micrographs of initial $C_{60}G_1$ (4.7×10^{-6} mol L^{-1}) on $2 \times 2 \mu m$ mica surface (a), mixing DNA with $C_{60}G_1$ at N/P = 2 for 30 min (b), and 180 min (c). [Color figure can be viewed in the online issue, which is available at wileyonlinelibrary.com.]

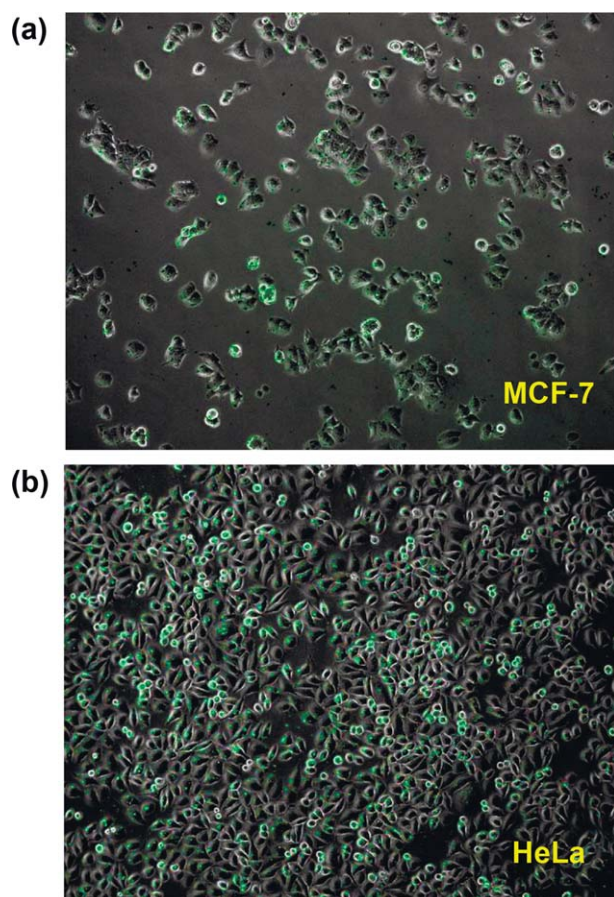


FIGURE 7. The overlaying optical and fluorescence microscope images for (a) MCF-7 and (b) HeLa cell lines internalized by $C_{60}G_1$ /DNA complexes at $N/P = 2$. The green spots represent a successful cellular uptake of YOYO-1-labeled DNA. [Color figure can be viewed in the online issue, which is available at wileyonlinelibrary.com.]

vectors. The CE_{50} value calculated from the linear correlation of relative fluorescence intensities at 605 nm versus the CE values was found to be only 1.3 [Fig. 5(b)], clearly confirming that amphiphilic $C_{60}G_1$ is an effective DNA binder. Barnard et al.³⁶ demonstrated the effective DNA binding of a family of amphiphilic dendrons bearing either long alkyl chains or cholesterol as the hydrophobic building blocks. The authors reported that self-assembled dendrons consistently achieved superior EtBr displacement, and had lower CE_{50} values, compared to non-self-assembled complexes. In our study, we found that a net positive charge of +4 per $C_{60}G_1$ molecule was insufficient to displace more than 50% of EtBr from its intercalation sites. However, the strong interaction of the hydrophobic C_{60} moiety is capable of inducing the close-packing of positively charged dendrons to form a C_{60} -based pseudodendrimer, by which DNA could be more efficiently wrapped into compact electrostatic complexes of a size that is suitable for cellular uptake. Additionally, gel electrophoresis analysis confirmed strong binding between $C_{60}G_1$ and DNA; more than 90% of DNA bound to C_{60} -based vectors at N/P ratios greater than 1.2 [Fig. 5(c)], consistent with our spectroscopic results.

AFM scanning was used to further visualize the morphology of the $C_{60}G_1$ and DNA complex at an optimized ratio of $N/P = 2$ to ensure complete binding between the vector and nucleic acids. Figure 6 shows micrographs of the as-formed complexes on a $2 \times 2 \mu\text{m}$ mica surface, confirming the electrostatic condensation of $C_{60}G_1$ with DNA, and clearly indicating a dynamic formation process. The small white dots in Figure 6(a) represent uniformly dispersed $C_{60}G_1$ nanoclusters; Figure 6(b) shows their partial aggregation into larger particles 30 min after mixing with pEGFP-C1 in water. At this stage, free $C_{60}G_1$ self-aggregates predominated over the DNA complexes, however, after standing for 3 h, the mixing solution exclusively contained the electrostatic DNA complexes, with an average diameter of approximately 140 nm, as determined by AFM section analysis [Fig. 6(c)]. DLS measurements also verified the dynamic formation process by revealing an increasing particle size distribution and narrowing polydispersity index, from 93 nm and 0.37, to 110 nm and 0.29, respectively. An optimized N/P ratio is a critical factor in DNA complex formation using polyamine-based vectors. Both AFM and DLS analyses suggested that extended complexation time benefit the formation of DNA/ $C_{60}G_1$ hybrid nanoparticles with favorable dimensions for cellular uptake.

Gene delivery into HeLa and MCF-7 cell lines

We performed a cellular uptake study using fluorescent YOYO-1 cyanine-based probes, which readily intercalate DNA with high binding affinity.³⁷ YOYO-1 does not emit fluorescence until bound to double-stranded DNA, when the emission intensity for these complexes dramatically

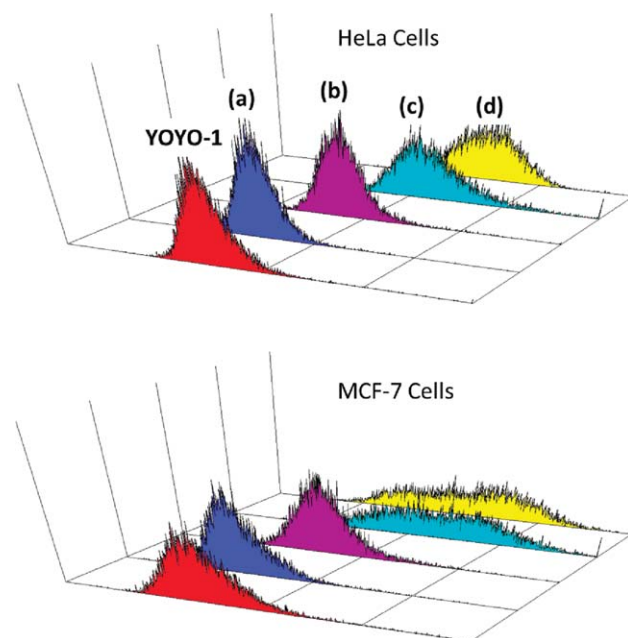


FIGURE 8. The flow cytometry histograms for counting 1×10^{-4} cells internalized by (a) DNA/YOYO-1, (b) $C_{60}G_1$ /YOYO-1, (c) TurboFect/DNA/YOYO-1, and (d) $C_{60}G_1$ /DNA/YOYO-1 complexes at $N/P = 2$. The incident laser wavelength was set to 488 nm. [Color figure can be viewed in the online issue, which is available at wileyonlinelibrary.com.]

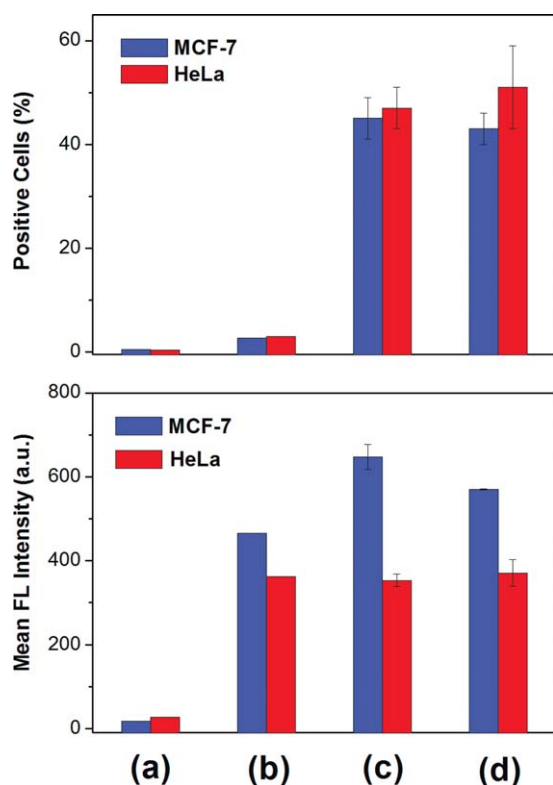


FIGURE 9. The quantitative analysis for flow cytometry in terms of positive cells and mean fluorescence intensity for cells internalized by (a) DNA/YOYO-1, (b) $C_{60}G_1$ /YOYO-1, (c) TurboFect/DNA/YOYO-1, and (d) $C_{60}G_1$ /DNA/YOYO-1 complexes at N/P = 2, where the concentrations of $C_{60}G_1$, DNA bases, and YOYO-1 are 1.51, 3.03, and 1.60×10^{-6} mol L $^{-1}$, respectively. [Color figure can be viewed in the online issue, which is available at wileyonlinelibrary.com.]

increases (Supporting Information Fig. S4). The fluorescence enhancement observed during the cellular uptake experiment confirmed the uptake of YOYO-1 labeled DNA, and allowed us to trace the *in vitro* and *in vivo* biodistributions of nucleic acids. To evaluate $C_{60}G_1$ -mediated gene delivery, pEGFP-C1 was pretreated with YOYO-1, followed by mixing with $C_{60}G_1$ at an N/P ratio of 2, to ensure complete association between DNA, vectors, and probe molecules. A commercially available transfection reagent (TurboFect) was used as a positive control for two cell lines—a breast cancer cell line, MCF-7 and a cervical cancer cell line, HeLa. Fluorescent microscopic images clearly show that the $C_{60}G_1$ /DNA complexes are taken up by both MCF-7 and HeLa cells (Fig. 7).

Flow cytometry analysis was performed to quantify the MCF-7 and HeLa cellular uptake efficiencies of $C_{60}G_1$ /DNA. Because the self-penetrating behavior of fluorescence dyes may affect the counting of positive cells, we used cells transfected by YOYO-1 alone as the negative control for the flow cytometry analysis. Notably, the result revealed YOYO-1 self-penetration into the target cell lines without the aid of a vector; and approximately 59% of HeLa cells were YOYO-1 positive, with weak mean fluorescence intensity of 48 units (Supporting Information Fig. S5). The flow histograms shown in Figure 8 indicate that the complex could be taken

up by both MCF-7 and HeLa cells, in agreement with the microscopic results. Figure 9 lists quantitative data in terms of the positive cells, and the mean fluorescence intensities for cells transfected by YOYO-1, DNA/YOYO-1 [Fig. 9(a)], $C_{60}G_1$ /YOYO-1 [Fig. 9(b)], TurboFect/DNA/YOYO-1 [Fig. 9(c)], and $C_{60}G_1$ /DNA/YOYO-1 complexes [Fig. 9(d)]. Comparing the two cell lines, we found that at an N/P ratio of 2, the overall uptake efficiency of $C_{60}G_1$ /DNA complexes toward HeLa cells was slightly greater than that for MCF-7 cells. Approximately 51% of HeLa cells were internalized by the $C_{60}G_1$ /DNA complexes, where the mean fluorescence intensity was 371 units, and approximately 43% of MCF-7 cells were positive to the complexes, with a mean fluorescence intensity of 570 units. These results suggest that using $C_{60}G_1$ assembly as a DNA vehicle is comparable to the TurboFect-mediated delivery system. We also performed a control experiment using amine-terminated G_2 PAMAM Dendron as the gene vector, and no cellular uptake was observed at the N/P value of 2 (Supporting Information Fig. S6). The G_2 dendron bears the same number of surface charges as $C_{60}G_1$, but lacks sufficient self-aggregation to deliver DNA into the target cells. Thus, the amphiphilic structure of $C_{60}G_1$ is crucial for gene delivery. Moreover, while comparing Figure 9(a,b), we found that approximately 3% of cells were internalized by YOYO-1 with remarkable fluorescence enhancement in the presence $C_{60}G_1$ (465 units for MCF-7 cells and 362 units for HeLa cells). Although the mechanism is unclear, we speculated that $C_{60}G_1$ is also capable of delivering rigid aromatic compounds into target cells.

CONCLUSION

Using a “pseudodendrimer” composed of amphiphilic dendrons as a nonviral gene vector, we developed a simple synthesis for a NH_2 -terminated PAMAM dendron-bearing fullereryl dyad through the CuAAC click reaction. The amphiphilic structure and solvophobic nature of C_{60} induce the dyad to form uniform core-shell-like nanoparticles in water. The polycationic C_{60} -based nanoparticles bind firmly with negatively charged pDNA at low N/P ratios, and both HeLa and MCF-7 cell lines readily take up the resulting electrostatic complexes. On the basis of the favorable binding affinity and cellular uptake obtained using C_{60} -based nanoparticles as carrier, investigations along gene transfection and EGFP expression are now underway and will be reported in due course.

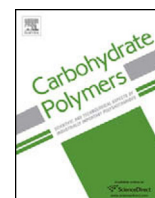
ACKNOWLEDGMENTS

NMR analysis was performed in the Instrument Center of Chung Shan Medical University, which is supported by the National Science Council, Ministry of Education, and Chung Shan Medical University.

REFERENCES

1. Tang MX, Redemann CT, Szoka FC. In vitro gene delivery by degraded polyamidoamine dendrimers. *Bioconjugate Chem* 1996; 7:703-714.

2. Navarro G, Tros de Ilarduya C. Activated and non-activated PAMAM dendrimers for gene delivery in vitro and in vivo. *Nano-medicine* 2009;5:287–297.
3. Yellepeddi VK, Kumar A, Palakurthi S. Biotinylated poly(amido amine) (PAMAM) dendrimers as carriers for drug delivery to ovarian cancer cells in vitro. *Anticancer Res* 2009;29:2933–2943.
4. Esfand R, Tomalia DA. Poly(amido amine) (PAMAM) dendrimers: From biomimicry to drug delivery and biomedical applications. *Drug Discov Today* 2001;6:427–436.
5. Menjoge AR, Kannan RM, Tomalia DA. Dendrimer-based drug and imaging conjugates: Design considerations for nanomedical applications. *Drug Discov Today* 2010;15:171–185.
6. Tomalia DA. Dendrons/dendrimers: Quantized, nano-element like building blocks for soft–soft and soft–hard nano-compound synthesis. *Soft Matter* 2010;6:456–474.
7. Rosen BM, Wilson CJ, Wilson DA, Peterca M, Imam MR, Percec V. Dendron-mediated self-assembly, disassembly, and self-organization of complex systems. *Chem Rev* 2009;109:6275–6540.
8. Russ V, Elfberg H, Thoma C, Kloeckner J, Ogris M, Wagner E. Novel degradable oligoethylenimine acrylate ester-based pseudodendrimers for in vitro and in vivo gene transfer. *Gene Ther* 2008;15:18–29.
9. Santos JL, Oliveira H, Pandita D, Rodrigues J, Pêgo AP, Granja PL, Tomás H. Functionalization of poly(amido amine) dendrimers with hydrophobic chains for improved gene delivery in mesenchymal stem cells. *J Controlled Release* 2010;144:55–64.
10. Yuba E, Nakajima Y, Tsukamoto K, Iwashita S, Kojima C, Harada A, Kono K. Effect of unsaturated alkyl chains on transfection activity of poly(amido amine) dendron-bearing lipids. *J Controlled Release* 2012;160:552–560.
11. Yu T, Liu X, Bolcato-Bellemin AL, Wang Y, Liu C, Erbacher P, Qu F, Rocchi P, Behr JP, Peng L. An amphiphilic dendrimer for effective delivery of small interfering RNA and gene silencing in vitro and in vivo. *Angew Chem Int Ed* 2012;51:8478–8484.
12. Guillot-Nieckowski M, Joester D, Stöhr M, Losson M, Adrian M, Wagner B, Kansy M, Heinzelmann H, Pugin R, Diederich F, Gallani JL. Self-assembly, DNA complexation, and pH response of amphiphilic dendrimers for gene transfection. *Langmuir* 2006;23:737–746.
13. Takahashi T, Kono K, Itoh T, Emi N, Takagishi T. Synthesis of novel cationic lipids having polyamidoamine dendrons and their transfection activity. *Bioconjugate Chem* 2003;14:764–773.
14. Guillot M, Eisler S, Weller K, Merkle HP, Gallani JL, Diederich F. Effects of structural modification on gene transfection and self-assembling properties of amphiphilic dendrimers. *Org Biomol Chem* 2006;4:766–769.
15. Bakry R, Vallant RM, Najam-ul-Haq M, Rainer M, Szabo Z, Huck CW, Bonn GK. Medicinal applications of fullerenes. *Int J Nanomed* 2007; 2: 639–649.
16. Cha C, Shin SR, Annabi N, Dokemci MR, Khademhosseini A. Carbon-based nanomaterials: Multifunctional materials for biomedical engineering. *ACS Nano* 2013;7:2891–2897.
17. Chen ML, He YJ, Chen XW, Wang JH. Quantum-dot-conjugate graphene as a probe for simultaneous cancer-targeted fluorescence imaging, tracking, and monitoring drug delivery. *Bioconjugate Chem* 2013;24:387–397.
18. Shen H, Zhang L, Liu M, Zhang, Z. Biomedical applications of graphene. *Theranostics* 2012;2:283–294.
19. Liu JH, Cao L, Luo PG, Yang ST, Lu F, Wang H, Meziani MJ, Haque SA, Liu Y, Lacher S, Sun YP. Fullerene-conjugated doxorubicin in cells. *ACS Appl Mater Interfaces* 2010;5:1384–1389.
20. Mamiya R, Noiri E, Isobe H, Nakanishi W, Okamoto K, Doi K, Sugaya T, Izumi T, Homma T, Nakamura E. In vivo gene delivery by cationic tetraamino fullerene. *PNAS* 2010;107:5339–5344.
21. Isobe H, Nakanishi W, Tomita N, Jinno S, Okayama H, Nakamura E. Gene delivery by aminofullerenes: Structural requirements for efficient transfection. *Chem-Asian J* 2006;1:167–175.
22. Isobe H, Sugiyama S, Fukui K, Iwasawa Y, Nakamura E. Atomic force microscope studies on condensation of plasmid DNA with functionalized fullerenes. *Angew Chem Int Ed* 2001;40:3364–3367.
23. Isobe H, Nakanishi W, Tomita N, Jinno S, Okayama H, Nakamura E. Nonviral gene delivery by tetraamino fullerene. *Mol Pharm* 2005;3:124–134.
24. Brettreich M, Burghardt S, Böttcher C, Bayerl T, Bayerl S, Hirsch A. Globular amphiphiles: Membrane-forming hexaadducts of C₆₀. *Angew Chem Int Ed* 2000;39:1845–1848.
25. Zhou S, Burger C, Chu B, Sawamura M, Nagahama N, Toganoh M, Hackler UE, Isobe H, Nakamura E. Spherical bilayer vesicles of fullerene-based surfactants in water: a laser light scattering study. *Science* 2001;291:1944–1947.
26. Burger C, Hao J, Ying Q, Isobe H, Sawamura M, Nakamura E, Chu B. Multilayer vesicles and vesicle clusters formed by the fullerene-based surfactant C₆₀(CH₃)₅K. *J Colloid Interface Sci* 2004;275:632–641.
27. Joester D, Losson M, Pugin R, Heinzelmann H, Walter E, Merkle HP, Diederich F. Amphiphilic dendrimers: novel self-assembling vectors for efficient gene delivery. *Angew Chem Int Ed* 2003;42:1486–1490.
28. Jones SP, Gabrielson NP, Pack DW, Smith DK. Synergistic effects in gene delivery—a structure–activity approach to the optimization of hybrid dendritic–lipidic transfection agents. *Chem Commun* 2008:4700–4702.
29. Posocco P, Pricl S, Jones S, Barnard A, Smith DK. Less is more—multiscale modelling of self-assembling multivalency and its impact on DNA binding and gene delivery. *Chem Sci* 2010;1:393–404.
30. Jones SP, Gabrielson NP, Wong CH, Chow HF, Pack DW, Posocco P, Fermeqlia M, Pricl S, Smith DK. Hydrophobically modified dendrons: developing structure–activity relationships for DNA binding and gene transfection. *Mol Pharm* 2011;8:416–429.
31. Meldal M, Tornøe CW. Cu-catalyzed azide-alkyne cycloaddition. *Chem Rev* 2008;108:2952–3015.
32. Srinivasachari S, Fichter KM, Reineke TM. Polycationic β -cyclodextrin “click clusters”: Monodisperse and versatile scaffolds for nucleic acid delivery. *J Am Chem Soc* 2008;130:4618–4627.
33. Chu CC, Tsai YJ, Hsiao LC, Wang LY. Controlled self-aggregation of C₆₀-anchored multiarmed polyacrylic acids and their cytotoxicity evaluation. *Macromolecules* 2011;44:7056–7061.
34. López AM, Scarel F, Carrero NR, Vázquez E, Mateo-Alonso A, Da Ros T, Prato M. Synthesis and characterization of highly water-soluble dendrofulleropyrrolidine bisadducts with DNA binding activity. *Org Lett* 2012;14:4450–4453.
35. Geall AJ, Blagbrough IS. Rapid and sensitive ethidium bromide fluorescence quenching assay of polyamine conjugate–DNA interactions for the analysis of lipoplex formation in gene therapy. *J Pharm Biomed Anal* 2000;22:849–859.
36. Barnard A, Posocco P, Pricl S, Calderon M, Haag R, Hwang ME, Shum VW, Pack DW, Smith DK. Degradable self-assembling dendrons for gene delivery: experimental and theoretical insights into the barriers to cellular uptake. *J Am Chem Soc* 2011;133:20288–20300.
37. Becker B, Clapper J, Harkins KR, Olson JA. In situ screening assay for cell viability using a dimeric cyanine nucleic acid stain. *Anal Biochem* 1994;221:78–84.



Synthesis of photoresponsive hybrid alginate hydrogel with photo-controlled release behavior



Chien-Ying Chiang^a, Chih-Chien Chu^{a,b,*}

^a School of Medical Applied Chemistry, Chung Shan Medical University, Taichung 40201, Taiwan

^b Department of Medical Education, Chung Shan Medical University Hospital, Taichung 40201, Taiwan

ARTICLE INFO

Article history:

Received 18 October 2014

Received in revised form

14 November 2014

Accepted 21 November 2014

Available online 28 November 2014

Keywords:

Alginate

Hydrogel

Azobenzene

Photoisomerization

Wound dressing

ABSTRACT

A photoresponsive hybrid alginate hydrogel was successfully prepared by Ca²⁺-mediated crosslinking reaction with a mixture of β-cyclodextrin-grafted alginate (β-CD-Alg) and diazobenzene-modified poly(ethylene glycol) (Az₂-PEG). The water-soluble Az₂-PEG exhibits efficient *trans*-to-*cis* isomerization of the terminal azobenzene moieties under UV-light irradiation and readily switched back to the initial *trans* state under visible light. Because of low affinity between β-CD and *cis*-Az, the host-guest inclusion complex formed by β-CD and *trans*-Az gradually dissociates under UV-light exposure. Accordingly, the bulk gel exhibits substantial photo-induced transformation in gel morphology by the appearance of significant comb-like cavities. This photosensitive behavior accompanied by the structural degradation enables the rapid release of entrapped dye molecules under UV light stimulus. Moreover, an incident light with higher power and mild acidic environment are capable of accelerating the photo-triggered release, thus allowing the potential applications toward acute wound healing.

© 2014 Elsevier Ltd. All rights reserved.

1. Introduction

Alginate, which is commonly isolated from brown algae, is an anionic linear polysaccharide composed of two saccharides: epimeric β-D-mannuronate (M) and α-L-guluronate (G). The M and G monomers are covalently bonded through 1,4-glycosidic linkages and arranged into either homopolymeric blocks (MM and GG) or alternating blocks (MGMG) along the polymeric backbone (Martins, Sarmiento, Souto, & Ferreira, 2007; Gattás-Asfura & Stabler, 2009; García-González, Alnaief, & Smirnova, 2011; Gong et al., 2011; Goh, Heng, & Chan, 2012). According to the “egg-box” model, two facing GG blocks can be coordinated with divalent Ca²⁺ ions, resulting in interchain crosslinking and hydrogel formation (Sikorski, Mo, Skjåk-Bræk, & Stokke, 2007; Coleman et al., 2011; Narayanan, Melman, Letourneau, Mendelson, & Melman, 2012; Cui et al., 2013).

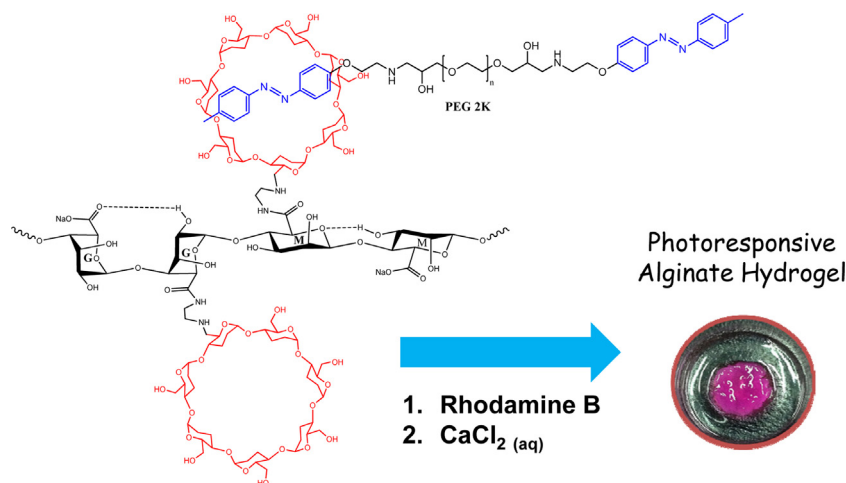
Alginate hydrogels have high water content, elasticity, and the ability to maintain a physiologically moist microenvironment in the wound bed; therefore, they are widely applied in tissue engineering (Patterson, Martino, & Hubbell, 2010; Sun & Tan, 2013; Bozza et al., 2014). Moreover, alginate wound dressings can

accommodate drugs and gradually release the drugs during the process of gel swelling to prevent wound infection (August, Kong, & Mooney, 2006; Bencherif et al., 2012; Pereira et al., 2013). However, alginates especially rich in GG blocks can incorporate more ionic interactions between chains and usually form a gel with high mechanical integrity. Therefore, during the controlled release of drugs, a bulk alginate hydrogel is less responsive to external stimuli such as temperature, pH level, and mechanical force. Recently, Han et al. (2012) presented a pH-sensitive shape-memory alginate hydrogel prepared by crosslinking a β-cyclodextrin (β-CD)-modified alginate and a diethylenetriamine-modified alginate. Ariga and co-workers reported a controlled release system containing a β-CD-crosslinked alginate gel triggered by a mechanical stimulus (Izawa et al., 2013). The release of drugs from this gel system was enhanced through mild mechanical compression because of a change in the host-guest inclusion ability of CD moieties for accommodating drug molecules.

Semiinterpenetrating networks (semi-IPNs) that are composed of one crosslinked polymer system in which free polymer chains are dissolved are capable of modulating the bulk properties of gel networks (Matricardi, Pontoriero, Coviello, Casadei, & Alhaique, 2008; Pescosolido et al., 2011). In semi-IPN systems, both crosslinked and free polymers synergistically contribute to the physicochemical properties of hybrid gels. Based on this concept, we developed a photoresponsive hybrid alginate semi-IPN that contains crosslinked β-CD-grafted alginate (β-CD-Alg) and

* Corresponding author at: School of Medical Applied Chemistry, Chung Shan Medical University, No. 110, Sec. 1, Jianguo N. Rd., Taichung 40201, Taiwan. Tel.: +886 4 2324 8189; fax: +886 4 2324 8189.

E-mail addresses: jrchu@csmu.edu.tw, jrchu3933@gmail.com (C.-C. Chu).



Scheme 1. Preparation protocol of a photoresponsive hybrid alginate hydrogel that contains crosslinked β -CD-grafted alginate (β -CD-Alg) and interpenetrating diazobenzene-terminated poly(ethylene glycol) (Az₂-PEG). Red-colored rhodamine B (RhB) is the mimic of entrapping drug molecules.

interpenetrating diazobenzene-terminated poly(ethylene glycol) (Az₂-PEG), as shown in Scheme 1. Because of the size and shape of the CD cavity, *trans*-Az and β -CD can form a favorable inclusion complex through host–guest affinity, whereas *cis*-Az is excluded from the complexation (Yuen & Tam, 2010; Tan et al., 2012). Therefore, the hybrid gel network features Ca²⁺ ions as cross-linkers as well as numerous junction points composed of β -CD and *trans*-Az inclusion complexes. Moreover, UV light irradiation induces efficient *trans*-to-*cis* isomerization (Peng, Tomatsu, & Kros, 2010; Tamesue, Takashima, Yamaguchi, Shinkai, & Harada, 2010; Meng et al., 2011). Accordingly, the hybrid alginate hydrogel is sensitive to the UV light used to facilitate *trans*-to-*cis* photoisomerization, which results in the dissociation of the inclusion complex and partial gel degradation. Thus, a light trigger can accelerate the release rate of small molecules entrapped within the gel. In addition to causing spontaneous drug release during gel swelling, this strategy entails using a bulk alginate hydrogel as a photocontrollable release system.

2. Experimental

2.1. General methods

All reactions were carried out under a nitrogen atmosphere. All solvents were dried following standard procedures. Sodium alginate ($M_w = 1.2\text{--}1.4 \times 10^5$ Da) and poly(ethylene glycol) diglycidyl ether ($M_n = 2 \times 10^3$ Da) were purchased from Sigma-Aldrich, and other chemical reagents were obtained as high-purity reagent-grade from commercial suppliers and used without further purification. Flash column chromatography was performed on spherical silica gel with 75–200 μm particle dimensions. ¹H (400 MHz) and ¹³C (100 MHz) NMR spectra were recorded on a Varian Mercury Plus 400 MHz spectrometer at room temperature. Spectral processing (Fourier transform, peak assignment and integration) was performed using MestReNova 6.2.1 software. *Trans/cis* photoisomerization for the azobenzene-containing polymers dissolved in organic solvents was carried out under the exposure of light-emitting diodes (LEDs) at 365 and 470 nm and an output power of 10 W. Ultraviolet–visible (UV–vis) absorption spectra were performed on a Thermo Genesys 10S UV–vis spectrometer equipped with a thermostatic cuvette holder. Field emission scanning electron microscopy (FE-SEM) was performed on a Jeol JSM-6700F instrument equipped with a cold-cathode field emission gun. The UV–vis measurement was carried out under a constant temperature. The relative viscosity (η_r) measurement was performed on

an Ostwald–Fenske viscometer using distilled water as a standard.

The hydrogel samples containing rhodamine B (RhB) with a strong fluorescence at $\lambda_{\text{max}} = 580$ nm were irradiated with 365 nm LED, and the reflective emission from the samples were collected and induced by a fiber bundle into a CCD imaging spectrometer (USB-4000, Ocean Optics) for the spectra recording. To carry out *trans*-to-*cis* photoisomerization, the samples were also excited by 365 nm LED for a specific time interval and in situ analyzed by the same experimental apparatus (see Fig. S1 in Supporting information).

2.2. Materials synthesis and characterization

2.2.1. Synthesis of (*E*)-4-(*p*-tolyl diazenyl)phenol (**1**)

An aqueous solution of NaNO₂ (1.91 g, 27.7 mmol) was slowly added into a solution of *p*-toluidine (1.52 g, 14.2 mmol) in 30 mL of 3 M HCl, and then the mixture was stirred under 0 °C for 30 min, followed by adding an aqueous buffer solution containing phenol (1.71 g, 18.2 mmol), NaOH (0.73 g, 18.2 mmol), and Na₂CO₃ (1.93 g, 18.2 mmol). After stirred at 0 °C for 30 min, the mixing solution was extracted by ethyl acetate for 3 times. The combined organic phase was dried over anhydrous magnesium sulfate, and rotary evaporation to dryness afforded the crude product. Further purification was performed on flash column chromatography (SiO₂, ethyl acetate/hexane = 2:8, $R_f = 0.4$) to yield the final product **1** as orange solid (2.41 g, 80%). ¹H NMR (400 MHz, CDCl₃): $\delta = 7.84$ (d, $J = 8.8$ Hz, 2H), 7.78 (d, $J = 8.3$ Hz, 2H), 7.29 (d, $J = 8.3$ Hz, 2H), 6.91 (d, $J = 8.8$ Hz, 2H), 5.74 (bs, 1H), 2.42 (s, 3H).

2.2.2. Synthesis of

(*E*)-1-(4-(2-bromoethoxy)phenyl)-2-(*p*-tolyl)diazene (**2**)

To a anhydrous THF solution of **1** (1.5 g, 7.1 mmol), K₂CO₃ (6.8 g, 49 mmol), and 18-crown-6 (20 g, 75 mmol), 1,2-dibromoethane (27 g, 0.14 mol) was added dropwisely over 30 min under N₂ atmosphere. The mixture was stirred at 45 °C for overnight and then extracted by ethyl acetate for 3 times. The combined organic phase was dried over anhydrous magnesium sulfate, and rotary evaporation to dryness afforded the crude product. Further purification was performed on flash column chromatography (SiO₂, ethyl acetate/hexane = 2:8, $R_f = 0.6$) to yield the final product **2** as orange solid (1.9 g, 84%). ¹H NMR (400 MHz, CDCl₃): $\delta = 7.90$ (d, $J = 9.1$ Hz, 2H), 7.79 (d, $J = 8.3$ Hz, 2H), 7.30 (d, $J = 8.3$ Hz, 2H), 7.01 (d, $J = 9.1$ Hz, 2H), 4.36 (t, $J = 6.3$ Hz, 2H), 3.67 (t, $J = 6.3$ Hz, 2H), 2.43 (s, 3H).

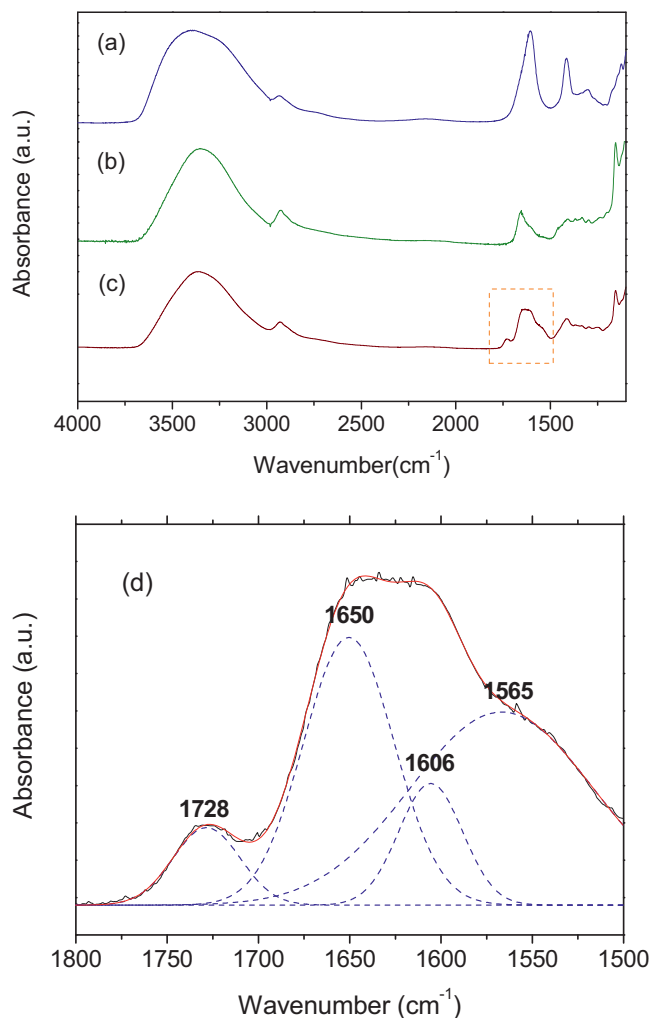


Fig. 1. FT-IR spectra of (a) sodium alginate, (b) mono-6-amino- β -CD, and (c) β -CD-Alg. (d) Peak deconvolution in the selected region shows the characteristic amide stretching at 1650 and 1565 cm^{-1} , and carboxylate stretching at 1606 cm^{-1} .

2.2.3. Synthesis of

(*E*)-1-(4-(2-azidoethoxy)phenyl)-2-(*p*-tolyl)diazene (**3**)

An anhydrous DMF solution of **2** (1.5 g, 4.7 mmol) and NaN₃ (3.2 g, 49 mmol) was stirred at 100 °C for overnight under N₂ atmosphere. The DMF was removed under vacuum, and then the mixture was extracted by ethyl acetate for 3 times. The combined organic phase was dried over anhydrous magnesium sulfate, and rotary evaporation to dryness afforded the final product **3** (1.1 g, 83%). ¹H NMR (400 MHz, CDCl₃): δ = 7.91 (d, J = 9.1 Hz, 2H), 7.79 (d, J = 8.3 Hz, 2H), 7.30 (d, J = 8.3 Hz, 2H), 7.02 (d, J = 9.1 Hz, 2H), 4.22 (t, J = 6.3 Hz, 2H), 3.64 (t, J = 6.3 Hz, 2H), 2.43 (s, 3H).

2.2.4. Synthesis of

(*E*)-2-(4-(*p*-tolyl)diazenyl)phenoxy)ethanamine (**Az**)

An anhydrous DMF solution of **3** (1.5 g, 5.3 mmol) and PPH₃ (6.3 g, 24 mmol) was stirred at room temperature for 2 h under N₂ atmosphere, followed by adding 5.3 mL of water and then stirred at 90 °C for another 3 h. The DMF was removed under vacuum, and then the mixture was extracted by ethyl acetate for 3 times. The combined organic phase was dried over anhydrous magnesium sulfate, and rotary evaporation to dryness afforded the crude product. Further purification was performed on flash column chromatography (SiO₂, methanol, R_f = 0.3) to yield the final product **Az** as orange solid (1.1 g, 81%). ¹H NMR (400 MHz, CDCl₃): δ = 7.90 (d, J = 9.0 Hz, 2H), 7.79 (d, J = 8.5 Hz, 2H), 7.29 (d, J = 8.5 Hz, 2H), 7.01 (d, J = 9.0 Hz,

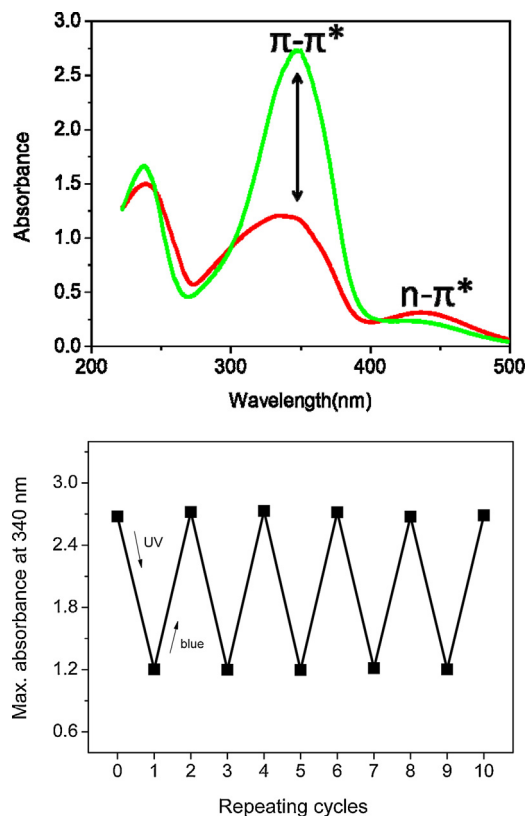


Fig. 2. (a) The absorbance change in π - π^* and n - π^* transitions of Az₂-PEG solution upon 365-nm LED excitation. (b) Reversible change in π - π^* absorbance by alternating 365-nm and 470-nm light irradiation.

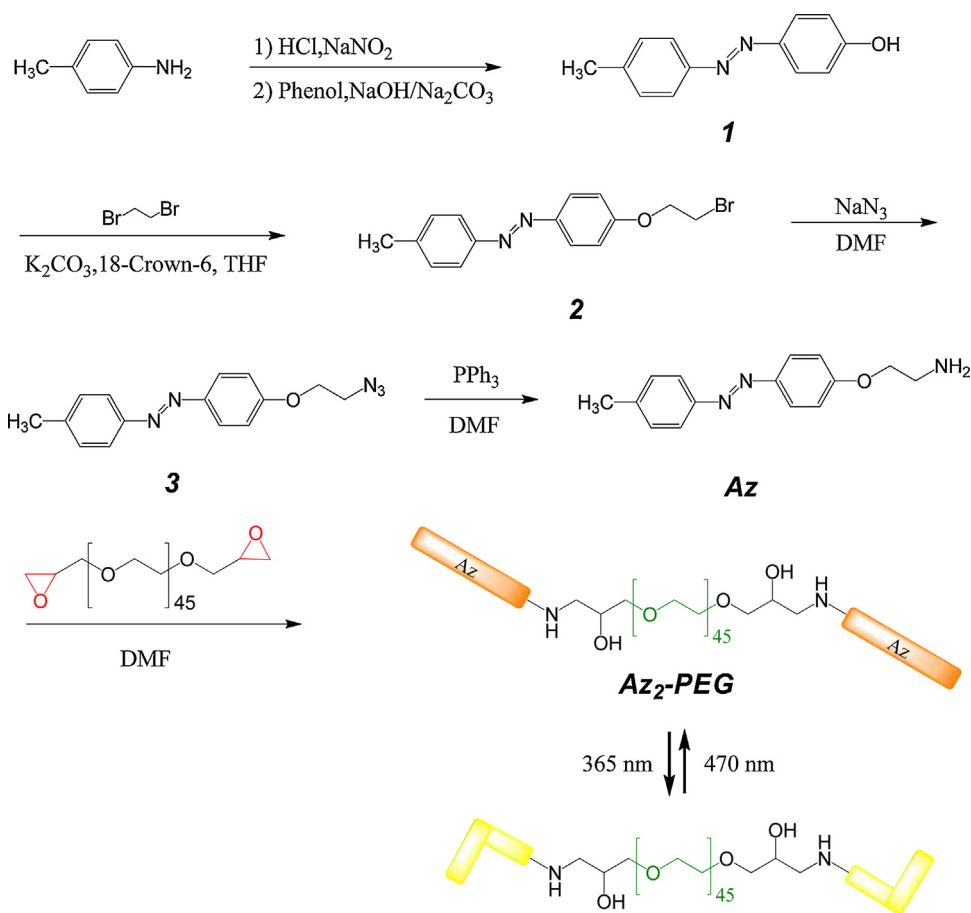
2H), 4.06 (t, J = 5.1 Hz, 2H), 3.12 (t, J = 5.1 Hz, 2H), 2.42 (s, 3H) 1.39 (bs, 2H).

2.2.5. Synthesis of diazobenzene-terminated poly(ethylene glycol) (Az₂-PEG)

An anhydrous DMF solution of **Az** (0.13 g, 0.51 mmol) and poly(ethylene glycol) diglycidyl ether (0.5 g, 0.25 mmol) was stirred at 100 °C under N₂ atmosphere until the complete disappearance of **Az**. The DMF was removed under vacuum, and then the mixture was extracted by ethyl acetate for 3 times. The combined organic phase was dried over anhydrous magnesium sulfate, and rotary evaporation to dryness afforded the crude product. Further purification was performed on flash column chromatography (SiO₂, methanol, R_f = 0.6) to yield the final product Az₂-PEG as dark-yellow solid (0.4 g, 80%).

2.2.6. Synthesis of β -cyclodextrin-grafted alginate (β -CD-Alg)

The mono-6-amino- β -CD was synthesized following the published procedure (Lin, Tsai, Tu, Jeng, & Chu, 2013). An aqueous buffer solution containing sodium alginate (108 mg, 2.4 mmol of COOH) and *N*-hydroxysuccinimide (1.61 g, 13.9 mmol) was slowly added by another aqueous solution of 1-(3-dimethylaminopropyl)-3-ethylcarbodiimide hydrochloride (2.67 g, 13.9 mmol). The reaction mixture was stirred at 4 °C for 10 min, followed by adding an aqueous solution of mono-6-amino- β -CD (2.82 g, 2.4 mmol). After reacting for another 12 h, the mixture was purified by membrane dialysis (molecular weight cut-off = 12,000–14,000 Da) against water for 3 days until complete removal of all the reagents, and lyophilization yields the final product as white powder. The ¹H NMR spectra are shown in Fig. S1. Based on the integral peak area (S1) of characteristic H-1 proton of β -CD (δ = 5.1 ppm) and the integral peak area (S2) of alginate protons from δ = 3.5–4.0 ppm,



Scheme 2. Synthetic route of diazobenzene-terminated poly(ethylene glycol) (Az_2 -PEG).

degree of substitution (DS) of β -CD along the polymer was determined following the relationship of $DS = (S1/7)/[(S2-4S1)/4]$ (Han et al., 2012).

2.2.7. Preparation of hybrid alginate hydrogel

An aqueous solution containing β -CD-Alg (15 mg), Az_2 -PEG (7 mg), and RhB (10^{-2} M, 0.5 mL) was blended thoroughly by vortex mixer, and the hydrogel was immediately formed as the mixture was added into 10% of CaCl₂ solution through a syringe. The bulk hydrogel was repeatedly rinsed with water until free red-colored dye molecules was completely removed from the gel network.

3. Results and discussion

Alginate polymers with varying degrees of β -CD substitution were first synthesized through carbodiimide-promoted amidation by using a commercially available sodium alginate and mono-6-amino- β -CD in various feeding ratios with respect to the carboxylate groups in a 2-(*N*-morpholino)ethanesulfonic acid (MES) buffer (pH=5.8) (Yang, Xie, & He, 2011). The resulting polymers were purified through dialysis to remove unreacted β -CD derivatives and then characterized using ¹H NMR and FT-IR analysis. Although the proton resonance exhibited by the polysaccharides on the β -CD ring and the alginate backbone substantially overlapped in the range of $\delta = 3.5 - 4.0$ ppm, the appearances of the characteristic anomeric protons at $\delta = 5.1$ ppm clearly indicated that β -CD was functionalized onto the alginate (Fig. S2) (Han et al., 2012; Izawa et al., 2013; Lin et al., 2013). Moreover, IR peak deconvolution in the selected region, confirming that an amide bond (I : 1650 and

II : 1565 cm⁻¹) joined the alginate and β -CD, and free carboxylate stretching was 1606 cm⁻¹ (Fig. 1).

The relative viscosity (η_r) measurement for 1 wt% aqueous solutions of pristine alginate and β -CD-Alg indicated that the η_r values of the polymer solutions decreased as the β -CD feeding ratios increased (Fig. S3). This result confirmed that β -CD-Alg with various β -CD grafting ratios was synthesized and that the dangling β -CD moieties along the alginate backbone effectively reduced the viscosity of the polymer solution. In preparing an alginate hydrogel, the viscosity of the alginate solution is critical, and therefore the degree of β -CD substitution was optimized. In addition, because the alginate crosslinking was mainly attributed to the coordination of Ca²⁺ ions with the carboxylate groups of two facing GG blocks, non-selective β -CD functionalization onto either M or G units exerted a substantial influence on the crosslinking property of the hydrogel. We discovered that higher β -CD grafting ratios along the backbone prohibited the crosslinking of each polymer chain and, thus, formed hydrogels may lose their mechanical integrity. Therefore, for preparing a crosslinkable hydrogel with a suitable mechanical strength, the feeding molar ratio of β -CD to the carboxylate groups were determined to be 1, and the average degree of substitution was approximately 0.17 according to NMR analysis.

The Az_2 -PEG, which acted as the second component in the semi-IPN gel system, was simply prepared through a substitution reaction of diepoxy PEG with amine-modified Az (Scheme 2). The photoisomerization of the Az molecules at PEG chain ends was analyzed using UV-vis absorption spectra. As shown in Fig. 2a, the decrease in $\pi-\pi^*$ absorbance from 2.6 to 1.2 at $\lambda_{max} = 340$ nm clearly confirmed that *trans*-to-*cis* isomerization occurred upon UV light irradiation, and alternating UV and visible light

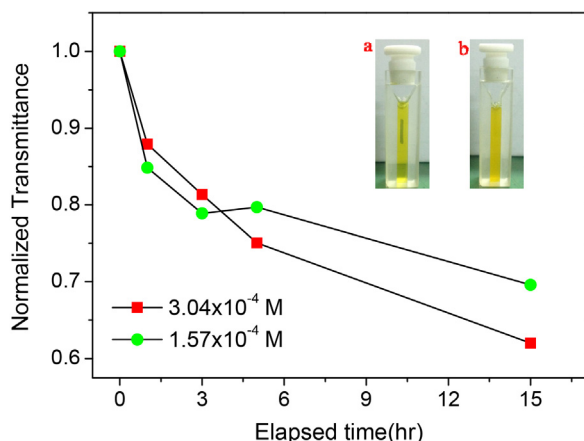


Fig. 3. The change in transmittance at $\lambda = 630$ nm for an aqueous mixture containing Az_2 -PEG and β -CD. The image shows a transparent solution (a) becomes opaque (b), indicating the formation of host–guest inclusion complex of these two components.

exposure resulted in a rapid, reversible photoswitch between the *trans* and *cis* states (Fig. 2b). Moreover, the host–guest reaction between Az_2 -PEG and β -CD was characterized according to the turbidity of the complex solution by using an incident beam at 630 nm (Ikeda, Ooya, & Yui, 1999). As shown in Fig. 3, the initial transparent solution became turbid after the two components were mixed for 1 h, and the transmittance decreased to approximately 65%. This result confirmed that inclusion complexes formed.

The hybrid alginate hydrogel was prepared through the drop-wise addition of the β -CD-Alg (15 mg/mL) and Az_2 -PEG (7 mg/mL) mixtures into an aqueous $CaCl_2$ solution. To mimic the release of small drug molecules, red-colored rhodamine B (RhB) with a strong fluorescence at $\lambda_{max} = 580$ nm was incorporated into the hybrid gel. Fig. 4a shows images and fluorescence spectra of an RhB-containing hydrogel stored in the dark. A slight decrease in fluorescence intensity within 60 min indicated the spontaneous release of RhB molecules into the surrounding water during gel swelling. Studies have reported that alginate hydrogels release hydrophobic curcumin molecules over a period of up to 20 days (Dai et al., 2009). By contrast, in the current study, the hybrid gel exhibited a substantial decrease in fluorescence intensity after 365-nm LED light irradiation, and it was almost colorless after UV light exposure for 60 min, as shown in Fig. 4b. Moreover, we examined the light-triggered release of a control hydrogel that contained only β -CD-Alg and RhB. Fig. 4c shows the results of a quantitative analysis of the change in fluorescence intensity of the control gel and hybrid gel systems upon light exposure. Only a slight decrease in the fluorescence intensity of the control gel precluded the photobleaching effect of RhB dyes produced through UV light irradiation and thus confirmed that the phototriggered rapid release of RhB molecules from the hybrid gel was successful. According to our thorough review of relevant research, this is the first report of the photocontrolled release of a bulk alginate hydrogel through a photoresponsive Az and β -CD inclusion complex.

We speculated that UV-light-induced *trans*-to-*cis* photoisomerization results in the dissociation of the host–guest complex of β -CD and *cis*-Az, thus agitating the IPN framework of the hybrid gel system. Consequently, the RhB molecules could be released from the bulk hydrogel more quickly upon UV light irradiation. As shown in Fig. 5a, our assumption was supported by two controlled experiments: (1) The release rate was increased by increasing the power of a UV lamp because more efficient photoisomerization yields more *cis* isomers; and (2) 470-nm LED light irradiation did not induce accelerated RhB release because *trans*-to-*cis* isomerization can be conducted only at a specific wavelength. In addition, we

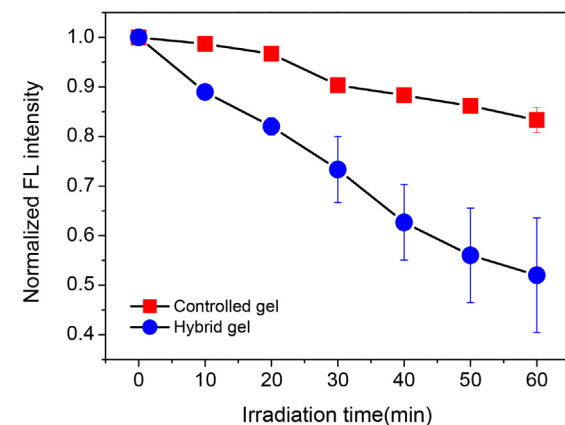
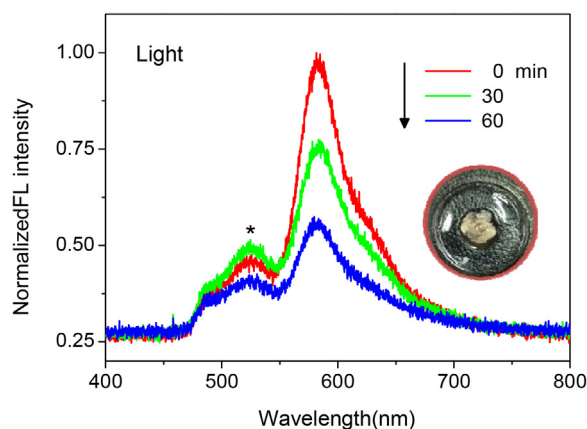
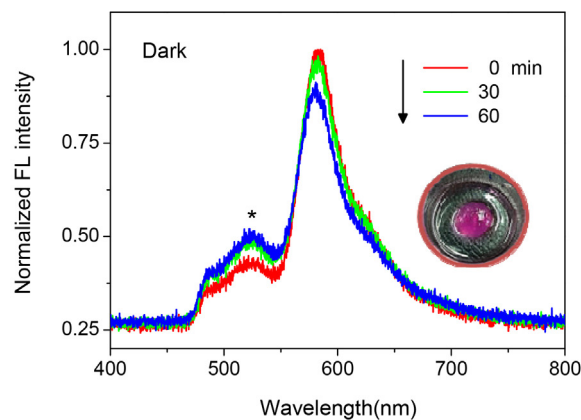


Fig. 4. Fluorescence spectra ($\lambda_{ex} = 365$ nm) and images of an RhB-containing hybrid hydrogel (a) stored in the dark and (b) upon UV-light exposure. (c) Quantitative analysis of the change in fluorescence intensity of the control gel (●) and hybrid gel (■). The control gel contains only β -CD-Alg and RhB.

compared hybrid hydrogels with contents of Az_2 -PEG ranging from 0.04 to 7 mg/mL. As shown in Fig. 5b, the release rate increased as the content of photoresponsive moieties increased, clearly suggesting that greater Az_2 -PEG contents engendered faster drug release upon UV light irradiation.

The change in the morphology of the photoresponsive hybrid hydrogels upon light stimulus was analyzed using scanning electron microscopy. Fig. 6a shows the β -CD-Alg hydrogel before and after UV light irradiation. The surface morphology was almost unchanged under light exposure, suggesting that the controlled hydrogel was insensitive to the UV light. This result confirmed that the accumulative heat during LED light exposure exerted no influence on the gel structure. Compared with a pristine Alg

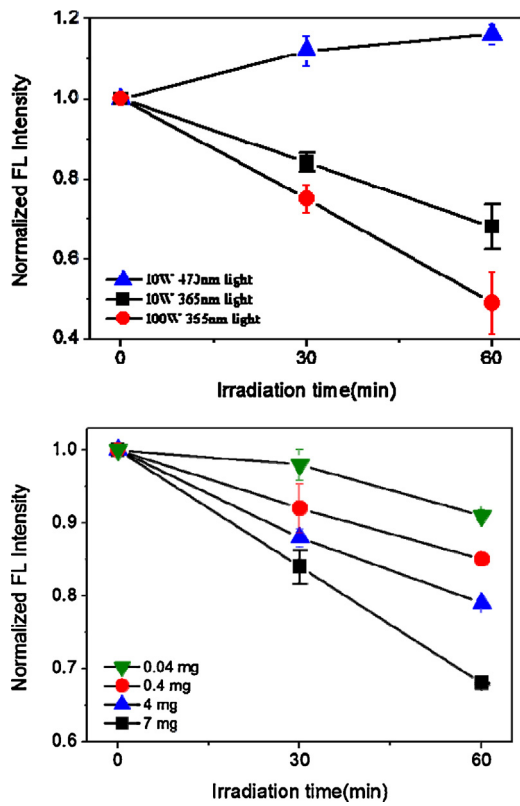


Fig. 5. (a) The change in fluorescence intensity of the hybrid hydrogels exposed to 365-nm light with lower (10 W) and higher (100 W) output energy and to 470-nm LED (10 W). (b) The change in fluorescence intensity of the hybrid hydrogels composed of an increasing amount of Az₂-PEG.

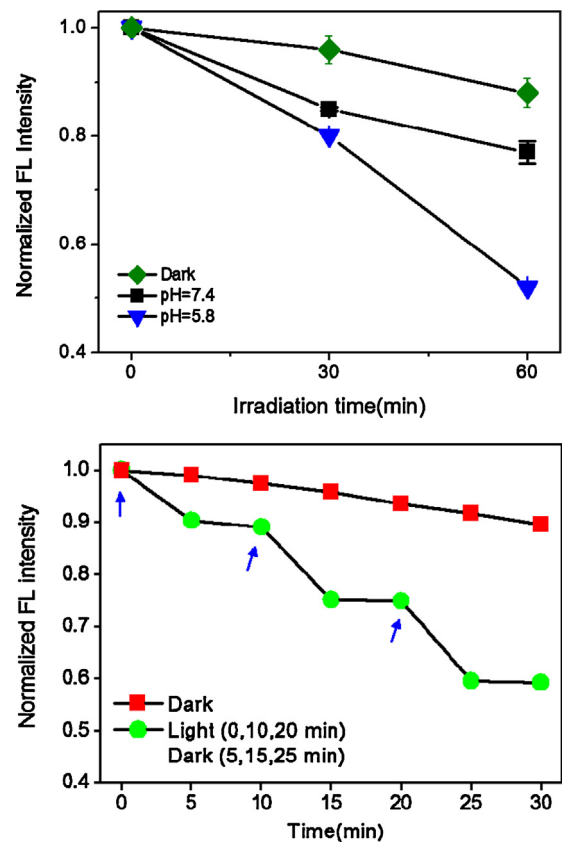


Fig. 7. (a) A pH-dependency of RhB releasing from hybrid hydrogel upon UV-light irradiation. (b) A stepped RhB releasing by alternating phototriggered and spontaneous processes. The hydrogel was irradiated with UV light at 0, 10, 20 min and exposed to darkness at 5, 15, 25 min.

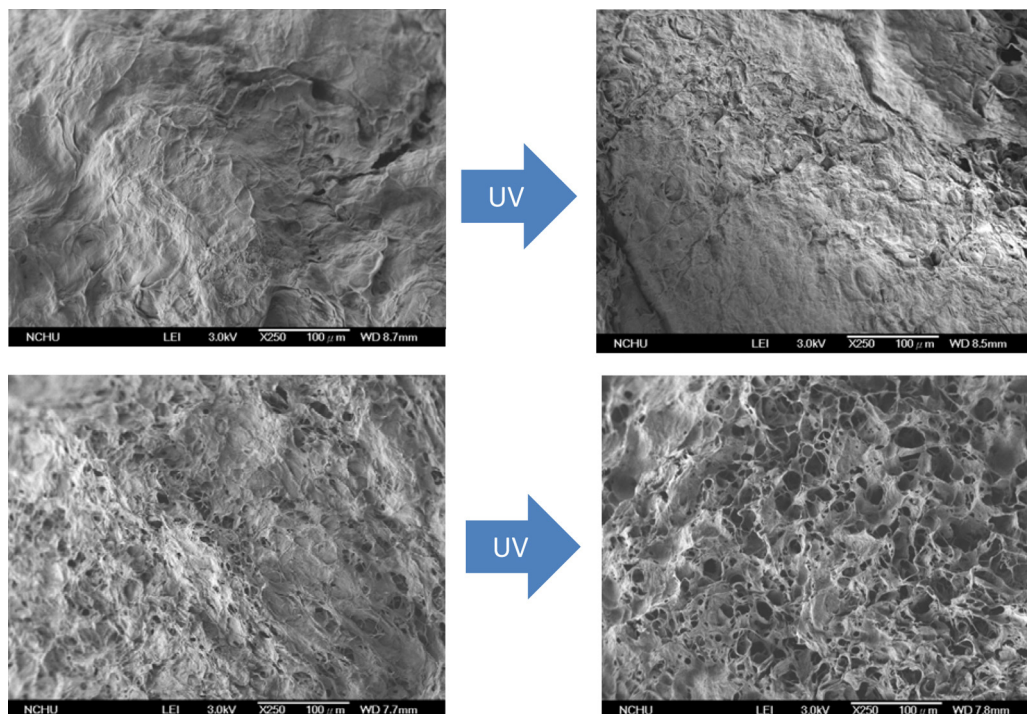


Fig. 6. Scanning electron microscopy (SEM) images of (a) β-CD-Alg hydrogel and (b) hybrid hydrogel before and after UV-light irradiation.

hydrogel exhibiting a smoother surface (Fig. S4), the structural integrity of the β -CD-Alg hydrogel with cracks on the surface was slightly lower. The loss of structural integrity may moderately enhance the release of RhB from the β -CD-modified hydrogel; this speculation is consistent with the fluorescence profile shown in Fig. 4c. Regarding the hybrid hydrogel system composed of Az₂-PEG and β -CD-Alg, Fig. 6b shows a substantial change in morphology upon UV light irradiation. The formation of comb-like cavities on the surface clearly indicated phototriggered structural degradation, which is mainly due to the photosensitive properties of the β -CD and Az inclusion complexes. Because of efficient *trans*-to-*cis* photoisomerization, the disassembly of *cis*-Az and β -CD may agitate the gel network, thus leading to a noticeable influence in structural integrity of the bulk hydrogel. Accordingly, gradual gel decomposition caused by UV light irradiation accounted for the accelerated release of entrapped RhB from the hybrid hydrogel.

In addition, the hybrid gel system exhibited pH dependency; the release rate in a mild acidic environment was greater than that in a physiological pH environment (Fig. 7a). Generally, both acute and chronic wounds gradually reach an acidic state as healing occurs (Tsukada, Tokunaga, Iwama, & Mishima, 1992; Gethin, 2007; Sikareepaisan, Ruktanonchai, & Supaphol, 2011). Therefore, this hybrid alginate hydrogel is applicable to photocontrollable delivery systems used in acute wound healing when rapid drug release is typically necessary. To provide a proof of concept of the photocontrolled accelerated release, the light exposure experiment was divided into three cycles repeated within 30 min. The hydrogel was irradiated with UV light for 5 min and then exposed to darkness for another 5 min. Fig. 7b shows a stepped release profile, according to which the RhB molecules were expeditiously released from the hydrogel after exposure to UV light but only gently released when the gel was exposed to darkness. This result suggested that alternating phototriggered and spontaneous release constitutes a well-controlled process and that rapid drug release in acute wound healing can be achieved through light stimulation.

4. Conclusion

In conclusion, we demonstrated a smart hybrid alginate hydrogel from which entrapped small molecules were rapidly released through UV light irradiation. The hybrid gel was prepared based on a semi-IPN structure composed of a crosslinked β -CD-grafted alginate and interpenetrating Az₂-PEG. In addition to crosslinking with the carboxylates along the alginate backbone induced by Ca²⁺ ions, the additional junctions formed by the host-guest complex between β -CD and *trans*-Az provided multiple photoresponsive sites within the bulk gel system. UV light irradiation induced efficient *trans*-to-*cis* photoisomerization, leading to the dissociation of the *cis*-Az from β -CD. Moreover, this photosensitive behavior was accompanied by substantial structural degradation of the hybrid gel, enabling the rapid release of entrapped molecules. Because biocompatible alginate hydrogels are widely applied in tissue engineering, *in vitro* and *in vivo* biological study of the applications of this photoresponsive hybrid gel in wound healing is currently being conducted.

Acknowledgement

The authors would like to thank the Ministry of Science and Technology of Taiwan (MOST102-2113-M-040-004) for financially supporting this research.

Appendix A. Supplementary data

Supplementary data associated with this article can be found, in the online version, at <http://dx.doi.org/10.1016/j.carbpol.2014.11.043>.

References

- August, A. D., Kong, H. J., & Mooney, D. J. (2006). Alginate hydrogels as biomaterials. *Macromolecular Bioscience*, 6, 623–633.
- Bencherif, S. A., Sands, R. W., Bhatta, D., Arany, P., Verbeke, C. S., Edwards, D. A., et al. (2012). Injectable preformed scaffolds with shape-memory properties. *Proceedings of the National Academy of Sciences of the United States of America*, 109, 19590–19595.
- Bozza, A., Coates, E. E., Incitti, T., Ferlin, K. M., Messina, A., Menna, E., et al. (2014). Neutral differentiation of pluripotent cells in 3D alginate-based cultures. *Biomaterials*, 35, 4636–4645.
- Coleman, R. J., Lawrie, G., Lambert, L. K., Whittaker, M., Jack, K. S., & Grøndahl, L. (2011). Phosphorylation of alginate: Synthesis, characterization, and evaluation of *in vitro* mineralization capacity. *Biomacromolecules*, 12, 889–897.
- Cui, J., Wang, M., Zheng, Y., Maria, G., Muñoz, R., & Campo, A. d. (2013). Light-triggered cross-linking of alginates with caged Ca²⁺. *Biomacromolecules*, 14, 1251–1256.
- Dai, M., Zheng, X., Xu, X., Kong, X., Li, X., Guo, G., et al. (2009). Chitosan-alginate sponge: Preparation and application in curcumin delivery for dermal wound healing in rat. *Journal of Biomedicine and Biotechnology*, 2009, 8.
- García-González, C. A., Alnaief, M., & Smirnova, I. (2011). Polysaccharide-based aerogels-promising biodegradable carriers for drug delivery systems. *Carbohydrate Polymers*, 86, 1425–1438.
- Gattás-Asfura, K. M., & Stabler, C. L. (2009). Chemoselective cross-linking and functionalization of alginate via Staudinger ligation. *Biomacromolecules*, 10, 3122–3129.
- Goh, C. H., Heng, P. W. S., & Chan, L. W. (2012). Alginates as useful natural polymer for microencapsulation and therapeutic applications. *Carbohydrate Polymers*, 88, 1–12.
- Gethin, G. (2007). The significance of surface pH in chronic wounds. *Wounds UK*, 3, 52–56.
- Gong, R., Li, C., Zhu, S., Zhang, Y., Du, Y., & Jiang, J. (2011). A novel pH-sensitive hydrogel based on dual crosslinked alginate/*N*- α -glutamic acid chitosan for oral delivery of protein. *Carbohydrate Polymers*, 85, 869–874.
- Han, X.-J., Dong, Z.-Q., Fan, M.-M., Liu, Y., Li, J.-H., Wang, Y.-F., et al. (2012). pH-induced shape-memory polymers. *Macromolecular Rapid Communications*, 33, 1055–1060.
- Ikedá, T., Ooya, T., & Yui, N. (1999). Regulation of pseudo-polyrotaxane formation between α -cyclodextrins and azobenzene-terminated poly(ethylene glycol). *Polymer Journal*, 31, 658–663.
- Izawa, H., Kawakami, K., Sumita, M., Tateyama, Y., Hill, J. P., & Ariga, K. (2013). β -Cyclodextrin-crosslinked alginate gel for patient-controlled drug delivery systems: Regulation of host-guest interactions with mechanical stimuli. *Journal of Materials Chemistry B*, 1, 2155–2161.
- Lin, Y. J., Tsai, B. K., Tu, C. J., Jeng, J., & Chu, C. C. (2013). Synthesis of β -cyclodextrin and poly(amido amine) dendron click cluster and its synergistic binding property. *Tetrahedron*, 69, 1801–1807.
- Martins, S., Sarmiento, B., Souto, E. B., & Ferreira, D. C. (2007). Insulin-loaded alginate microspheres for oral delivery-effect of polysaccharide reinforcement on physicochemical properties and release profile. *Carbohydrate Polymers*, 69, 725–731.
- Matricardi, P., Pontoriero, M., Coviello, T., Casadei, M. A., & Alhaique, F. (2008). *In situ* cross-linkable novel alginate-dextran methacrylate IPN hydrogels for biomedical applications: Mechanical characterization and drug delivery properties. *Biomacromolecules*, 9, 2014–2020.
- Meng, X.-W., Ha, W., Cheng, C., Dong, Z.-Q., Ding, L.-S., Li, B.-J., et al. (2011). Hollow nanospheres based on the self-assembly of alginate-grafted-poly(ethylene glycol) and alpha-cyclodextrin. *Langmuir*, 27, 14401–14407.
- Narayanan, P. P., Melman, G., Letourneau, N. J., Mendelson, N. L., & Melman, A. (2012). Photodegradable iron(III) cross-linked alginate gels. *Biomacromolecules*, 13, 2465–2471.
- Patterson, J., Martino, M. M., & Hubbell, J. A. (2010). Biomimetic materials in tissue engineering. *Materials Today*, 13.
- Peng, K., Tomatsu, I., & Kros, A. (2010). Light controlled protein release from a supramolecular hydrogel. *Chemical Communications*, 46, 4094–4096.
- Pereira, R., Carvalho, A., Vaz, D. C., Gil, M. H., Mendes, A., & Bártolo, P. (2013). Development of novel alginate based hydrogel films for wound healing applications. *International Journal of Biological Macromolecules*, 52, 221–230.
- Pescosolido, L., Vermonden, T., Malda, J., Censi, R., Dhert, W. J. A., Alhaique, F., et al. (2011). *In situ* forming IPN hydrogels of calcium alginate and dextran-HEMA for biomedical applications. *Acta Biomaterialia*, 7, 1627–1633.
- Sikareepaisan, P., Ruktanonchai, U., & Supaphol, P. (2011). Preparation and characterization of asiaticoside-loaded alginate films and their potential for use as effectual wound dressings. *Carbohydrate Polymers*, 83, 1457–1469.
- Sikorski, P., Mo, F., Skjåk-Bræk, G., & Stokke, B. T. (2007). Evidence for egg-box-compatible interactions in calcium-alginate gels from fiber X-ray diffraction. *Biomacromolecules*, 8, 2098–2103.

- Sun, J., & Tan, H. (2013). Alginate-based biomaterials for regenerative medicine applications. *Materials*, *6*, 1285–1309.
- Tamesue, S., Takashima, Y., Yamaguchi, H., Shinkai, S., & Harada, A. (2010). Photoswitchable supramolecular hydrogels formed by cyclodextrins and azobenzene polymers. *Angewandte Chemie International Edition*, *49*, 7461–7464.
- Tan, L., Liu, Y., Ha, W., Ding, L.-S., Peng, S.-L., Zhang, S., et al. (2012). Stimuli-induced gel–sol transition of multi-sensitive supramolecular β -cyclodextrin grafted alginate/ferrocene modified pluronic hydrogel. *Soft Matter*, *8*, 5746–5749.
- Tsukada, K., Tokunaga, K., Iwama, T., & Mishima, Y. (1992). The pH changes of pressure ulcers related to the healing process of wounds. *Wounds*, *4*, 16–20.
- Yang, J.-S., Xie, Y.-J., & He, W. (2011). Research progress on chemical modification of alginate: A review. *Carbohydrate Polymers*, *84*, 33–39.
- Yuen, F., & Tam, k. C. (2010). Cyclodextrin-assisted assembly of stimuli-responsive polymers in aqueous media. *Soft Matter*, *6*, 4613–4630.

trans/cis-Isomerization of Fluorene-Bridged Azo Chromophore with Significant Two-Photon Absorbability at Near-Infrared Wavelength

Chih-Chien Chu,^{*,[a, b]} Ya-Chi Chang,^[a] Bo-Kai Tsai,^[c] Tzu-Chau Lin,^[c] Ja-Hon Lin,^[d] and Vincent K. S. Hsiao^[e]

Abstract: Azo-containing materials have been proven to possess second-order nonlinear optical (NLO) properties, but their third-order NLO properties, which involves two-photon absorption (2PA), has rarely been reported. In this study, we demonstrate a significant 2PA behavior of the novel azo chromophore incorporated with bilateral diphenylaminofluorenes (DPAFs) as a π framework. The electron-donating DPAF moieties cause a redshifted π - π^* absorption band centered at 470 nm, thus allowing efficient blue-light-induced *trans*-to-*cis* photoisomerization with a rate constant of $2.04 \times 10^{-1} \text{ min}^{-1}$ at the photostationary state (PSS). The open-aperture Z-scan technique that adopted a femtosecond (fs) pulse laser as excitation source shows an appreciably higher 2PA cross-section for the fluorene-derived azo chromophore than that for common azobenzene dyes at near-infrared wavelength ($\lambda_{\text{ex}} = 800 \text{ nm}$). Furthermore, the fs 2PA response is quite uniform regardless of the molecular geometry. On the basis of the computational modeling, the intramolecular charge-transfer (ICT) process from peripheral diphenylamines to the central azo group through a fluorene π bridge is crucial to this remarkable 2PA behavior.

Azobenzene (azo) chromophores have been incorporated into a wide variety of molecular architectures including polymers, dendrimers, liquid crystals, self-assembled monolayers, and biomaterials.^[1] Azo chromophores undergo a uniquely clean and efficient photoisomerization; they ex-

hibit facile geometric isomerization between their *trans* and *cis* forms.^[2] Generally, *trans*-azobenzene shows intense π - π^* absorption in the UV region, and noncoherent UV light can rapidly induce the *trans*-to-*cis* isomerization. The *cis* isomer has an enhanced n - π^* absorption in the visible region; thus, the *trans* isomers are regenerated from the *cis* state through visible-light irradiation. Accordingly, *trans/cis* azobenzenes can be readily switched by alternating UV and visible-light exposure. This light-induced interconversion allows the system that incorporates azo chromophores to be applied in phototriggered molecular switches and machines.^[3] With electron donor-acceptor (D-A) ring substitution, azo chromophores have been extensively studied for second-order nonlinear optical (NLO) applications.^[4] Irradiation in the absorption band of poled azo polymers with a pulse laser beam, for example, can cause significant second-harmonic generation (SHG) decay correlated with *trans*-to-*cis* isomerization, followed by a rapid recovery to the initial SHG level when the *cis* isomer thermally relaxes back to the *trans* state.^[5] This marked photoswitching of the “on/off” SHG signal is mainly attributed to the distinctive hyperpolarizability of *trans* and *cis* azobenzenes. A more π -conjugated *trans* isomer has a higher hyperpolarizability, thus enabling the NLO response to be more readily switched between the *trans* and *cis* states.

Recently, third-order NLO behavior that involves a two-photon absorption (2PA) process has drawn considerable attention because of many promising applications in the emerging fields of photonics and biophotonics, including optical power limiting, 3D data storage, 3D microfabrication, bioimaging and tracking, and 2PA-assisted photodynamic therapy.^[6] The 2PA efficiency, namely, the 2PA cross-section for the organic chromophores, is, in general, closely related to both the intramolecular charge-transfer (ICT) efficiency in D- π -D-, A- π -A-, and D- π -A-type structures and the effective π -conjugation length within a molecule.^[7] The π bridges, similar to a highly rigid fluorene unit, provide delocalization and conjugation, which are critical for increasing the 2PA cross-section. Moreover, elongation of the π frameworks through either alkenyl (C=C) or alkynyl (C \equiv C) linkages also results in extension of the effective π -conjugation length and, thus, the enhancement of 2PA efficiency. However, use of an azo moiety (N=N) as the conjugation linkage to achieve the 2PA process has been rarely reported.^[8] Antonov et al. conducted a systematic study on the 2PA cross-

[a] Prof. Dr. C.-C. Chu, Y.-C. Chang
School of Medical Applied Chemistry,
Chung Shan Medical University, South District, Taichung (Taiwan)
E-mail: jrchu@csmu.edu.tw

[b] Prof. Dr. C.-C. Chu
Department of Medical Education
Chung Shan Medical University Hospital, Taichung 40201 (Taiwan)

[c] B.-K. Tsai, Prof. Dr. T.-C. Lin
Department of Chemistry
National Central University, Jhong-Li 32001 (Taiwan)

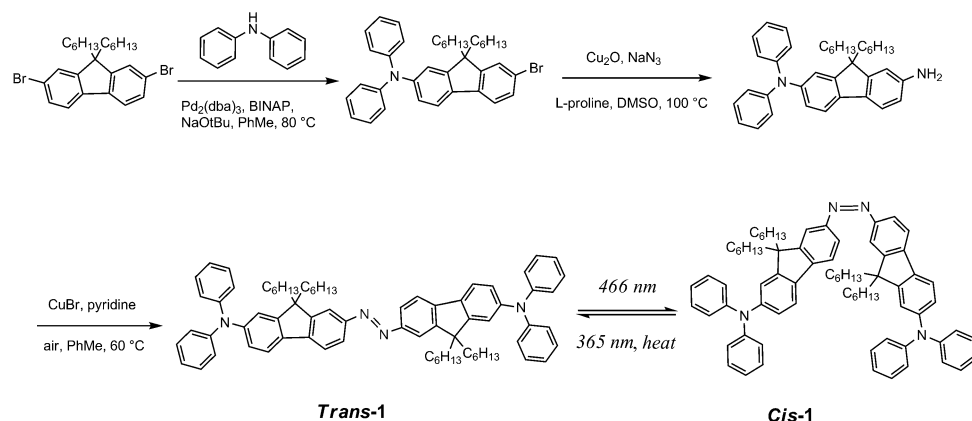
[d] Prof. Dr. J.-H. Lin
Department of Electro-Optical Engineering
National Taipei University of Technology, Taipei 10608 (Taiwan)

[e] Prof. Dr. V. K. S. Hsiao
Department of Applied Materials and Optoelectronic Engineering
National Chi Nan University, Puli 54561 (Taiwan)

Supporting information for this article is available on the WWW under <http://dx.doi.org/10.1002/asia.201402896>.

sections in several D- π -A-type azoaromatic compounds and suggested that the strength of the donor and/or acceptor groups is significant.^[8a] Furthermore, Magennis et al. demonstrated a 2PA photochromism in a commercial azo chromophore. The *trans*-to-*cis* isomerization could be performed using two-photon excitation by employing 740 nm femtosecond (fs) laser pulses.^[8b] Consequently, we envisioned that the third-order 2PA behavior of azo-containing materials proven to possess a second-order NLO property should be explored further.

As a proof-of-concept for this study, we synthesized a D- π -D compound **1**, in which two electron-donating diphenylaminofluorenes (DPAFs) were directly linked by an azo group, to examine the correlation between *trans/cis* photoisomerization and 2PA properties. As shown in Scheme 1, symmetric azo compound **1**, indicated in deep orange, was successfully synthesized by homocoupling two 2-amino-substituted DPAF through a copper-catalyzed aerobic oxidative dehydrogenative process.^[9] This symmetric azo-coupling reaction was executed under mild conditions, using copper bromide as the catalyst and air as the oxidant. The excellent yield in this reaction was attributed to the electron-donating character of the diphenylamine substituents. Thin-layer chromatography (TLC) analysis, using an ethyl acetate and hexane mixture (1:19) as the eluent, showed a single composition for compound **1** at $R_f=0.83$, thus indicating clearly a geometric state of either pure *trans* or pure *cis* form. The proton and carbon peaks shown in the ¹H and ¹³C NMR spectra also confirmed the existence of compound **1** as



Scheme 1. Synthetic route for azo compound **1** bearing bilateral electron-donating diphenylaminofluorenes (DPAFs).

a single component (see the Supporting Information). However, neither method could determine the *trans* and *cis* geometries. Research has shown that *trans* and *cis* azobenzenes can be distinguished according to their characteristic Raman shifts.^[10] Therefore, we adopted micro-Raman spectroscopy to analyze directly the vibrational spectrum of a solid sample. Figure 1a shows the Raman spectra for compound **1** based on using a 633 nm He:Ne laser as the excitation source. The Raman shifts centered at 1142 (CN stretch),

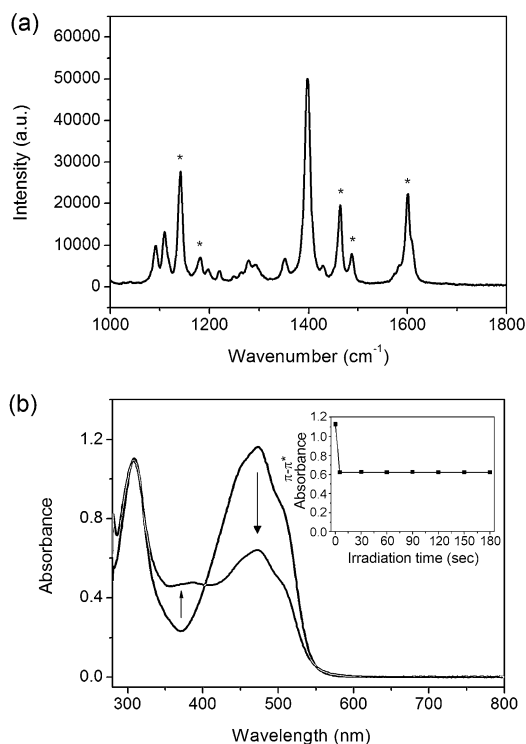


Figure 1. a) Micro-Raman spectroscopic analysis for azo compound **1**. The marked peaks denote the characteristic vibration modes of the *trans* isomer. b) UV-visible spectroscopic analysis for *trans* **1** upon 466 nm LED irradiation. The inset shows the maximum decrease in π - π^* absorbance within 5 s exposure time.

1182 (CN stretch), 1464 (NN stretch), 1487 (NN stretch), and 1600 cm^{-1} (CC stretch) were characteristic vibrations of *trans* azobenzene, thus indicating that compound **1** was a thermodynamically stable *trans* product. Moreover, the absence of the in-plane ring bending mode at approximately 1440 cm^{-1} might indicate the rigidity of azo compound **1** based on the fluorene framework.

Compared with *trans* aromatic azo compounds that have an intense π - π^* absorption in the UV region, *trans* compound **1** (Figure 1b), with bilateral

electron-donating DPAF moieties, showed a broad and intense absorption band in the visible region centered at approximately 470 nm (with a molar extinction coefficient of ϵ at approximately $4.5 \times 10^4 \text{ M}^{-1} \text{ cm}^{-1}$). This redshifted band, with a coplanar *trans* configuration, suggested that compound **1** had an elongating π -conjugation length and a lower bandgap energy of π - π^* transition. Therefore, *trans*-to-*cis* photoisomerization for azo compound **1** was expected to transpire under the excitation of visible light instead of UV

light. A first attempt that involved using a 467 nm argon ion laser (approximately 30 mW) as the excitation source could not produce any change in π - π^* absorbance, thus indicating that compound **1** remained in the all-*trans* state. For performing the *trans*-to-*cis* photoisomerization, a higher radiant flux and a larger incident beam exposure area were introduced by employing a noncoherent light-emitting diode (LED) with a higher output energy (approximately 10 W) and a maximum blue emission of 466 nm. As shown in Figure 1b, on LED irradiation, absorbance at 470 nm rapidly reduced within several seconds and remained at a constant value for a longer exposure time. This partial decrease in absorbance was apparently due to the formation of a *cis* product with a relatively poor π -conjugation system and blue-shifted π - π^* absorption. The light-induced isomerization for a dilute solution of aromatic azo compounds generally results in either an all-*trans* or an all-*cis* photostationary state (PSS). However, the PSS for compound **1**, established through blue LED irradiation and readily visualized using normal-phase TLC analysis, was composed of both *trans* and *cis* products. The R_f value of the *cis* isomer (0.55) was lower than that of the *trans* isomer (0.83), consistent with the fact that *cis* isomers possess a significant dipole moment and higher polarity. On the assumption that *cis* **1** would be completely transparent at 470 nm, *cis* content was calculated on the basis of a drop in blue-light absorbance of approximately 45% during LED irradiation; the *trans* isomer was the component in slight excess in this isomeric mixture.

In addition to a decrease in π - π^* absorbance, we observed an increasing absorption band in the UV region of 350–400 nm. We speculated that this increasing band corresponded to the π - π^* absorption of the *cis* isomer. Because the 2-amino-substituted DPAF precursor possessed intense UV absorption centered at 330 nm (with a molar extinction coefficient of ϵ at approximately $2.2 \times 10^4 \text{ M}^{-1} \text{ cm}^{-1}$) and because the *cis* isomer possessed a poor π conjugation on the central N=N bond, the *cis* isomer was expected to have a blue-shifted π - π^* absorption band in the UV region. As indicated by this UV absorption band, the *cis* isomer could be switched back to the *trans* form with a 365 nm LED light. As shown in Figure 2a, the absorbance returned to its initial UV irradiation values within several seconds, and the *trans/cis* isomerization in solutions in both toluene and THF could be reversibly switched by alternating UV and blue-light irradiation. The photoisomerization of compound **1** manifested a notable difference from conventional azobenzene systems in that it possessed a reverse direction of the photoswitching wavelengths: a *trans*-to-*cis* interconversion with visible (blue) light but a *cis*-to-*trans* back-isomerization with UV light.

One- and two-dimensional ^1H NMR spectra of compound **1** (approximately 10^{-2} M in CDCl_3) from alternating visible and UV-light irradiation were compared (see the Supporting Information). Figure 2b shows the partial spectrum for symmetric all-*trans* **1** and the marked aromatic resonances, with H^1 and H^2 denoting the *ortho* protons adjacent to the N=N bond. The complexity of the aromatic protons after blue-

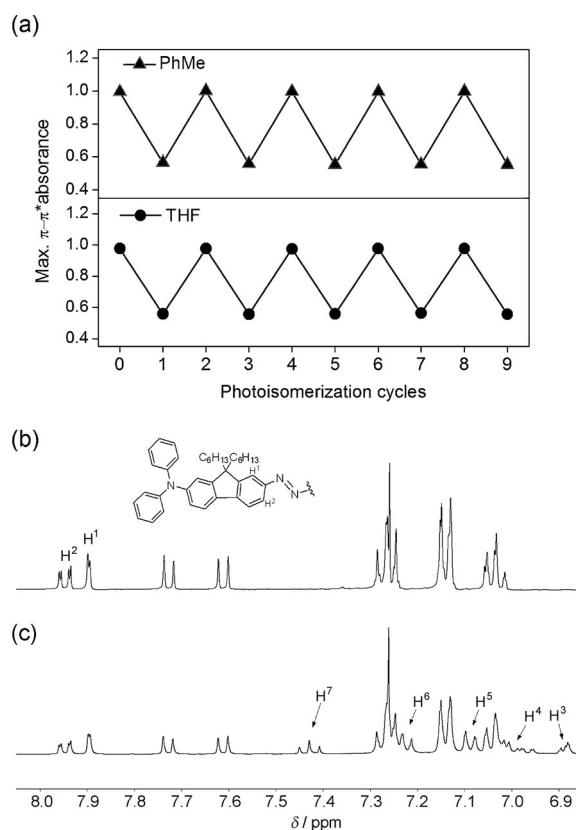


Figure 2. a) Reversible photoswitch for azo compound **1** upon alternating blue- and UV-light irradiation. ^1H NMR spectroscopic analysis for b) all-*trans* **1**, and c) *trans/cis*-isomeric mixture by blue-light irradiation for 10 min. H^1 and H^2 denote the characteristic *ortho* protons adjacent to the N=N bond of *trans* isomer; H^3 – H^7 denote the aromatic protons of *cis* isomer.

light irradiation, which ranged from $\delta = 6.9$ to 7.3 ppm, indicated the existence of both *trans* and *cis* products (Figure 2c). The distinguishable peaks of H^3 to H^7 denoted the characteristic protons on the *cis* structure. The integral area of the spectrum from H^7 to either H^1 or H^2 gradually increased as the light exposure time was extended, thereby suggesting that the *cis* content in the isomeric mixture could be increased with a longer irradiation time. On the basis of the integral ratios between the typical protons of these two isomers, the calculated maximum *cis* content was approximately 30–40% under NMR spectroscopic experimental conditions. Moreover, after UV-light irradiation, all of the *cis* isomers were switched back to the *trans* form; thus, the obtained NMR spectrum was identical to the original spectrum of all-*trans* **1**. NMR spectroscopic and UV/Vis absorption analyses confirmed an efficient and reversible *trans/cis* photoswitching of this fluorene-based azo compound in concentrated and dilute solutions, respectively.

The PSS for compound **1**, established through blue-light irradiation, contained both *trans* and *cis* isomers at a fixed ratio; further irradiation did not increase the *cis* content. The approach of the PSS is attributed to equal reaction rates of forward (*trans*-to-*cis*) and backward (*cis*-to-*trans*) in-

terconversions under 466 nm LED excitation. We assumed that the incomplete transformation was due to an increase in the backward reaction rate during light exposure and was dominated by two main factors. The first factor was the rapid thermal relaxation of the *cis* isomer to the thermodynamic *trans* product. Following the first-order kinetic shown in the Supporting Information, the thermal isomerization rate (k_t) calculated according to the recovery of π - π^* absorbance at room temperature was determined to be $1.13 \times 10^{-2} \text{ min}^{-1}$, approximately 20-fold faster than common azobenzenes, such as 4-butyl-4'-methoxyazobenzene ($5.80 \times 10^{-4} \text{ min}^{-1}$).^[11] The more likely cause for the increasing backward thermal isomerization of *cis* **1** was the destabilization of the N=N bond by the bilateral electron-donating DPAF moieties.^[12] Secondly, the *cis* isomer might have undergone a symmetry-allowed n - π^* transition in the visible region to cause the π - π^* and n - π^* transitions of *trans* and *cis* isomers, respectively, to possess similar energy gaps. Once the isomeric system contained certain amounts of *cis* isomers, blue-light irradiation induced the photoisomerization in both directions simultaneously. Thus, the equilibrium state was soon reached because of an accelerating backward reaction. We then employed high-performance liquid chromatography (HPLC) to separate the *trans* and *cis* isomers quickly and verify their UV/Vis absorption spectra through on-line photodiode array (PDA) detection. The HPLC chromatograms revealed two well-resolved peaks, the *trans* product at 2.9 min and the *cis* product at 3.1 min (Figure 3a). The increase in the integral ratio of *cis/trans* peaks under different light exposure times also confirmed that the *cis* content gradually increased until the PSS was reached. The absorption profile of *trans* **1** obtained from PDA detection in Figure 3b agreed with the UV/Vis spectrum shown in Figure 1b. Two distinct absorption bands for *cis* **1** were noticed in the UV and visible regions, which presumably corresponded to the π - π^* and n - π^* electronic transitions, respectively. Because of the overlap of the π - π^* and n - π^* absorption for *trans* and *cis* isomers, respectively, backward *cis*-to-*trans* photoisomerization was also promoted under blue-light excitation. On the basis of the same molar extinction coefficients of *trans* and *cis* **1** at 300 nm (Figure 3b), the calculation of the integral areas for the two isomers from the chromatograms at this detection wavelength suggested a maximum *cis* content of 35%.

The irradiation time course of the *cis* contents was also established by using NMR spectroscopy to obtain the rate constant of k_p at PSS with a blue-light exposure. The experimental data fit the rate law well and yield the values of *cis* content (at PSS) = 36.3% and $k_p = 2.04 \times 10^{-1} \text{ min}^{-1}$ (Figure 3c).^[8b] Considering that k_p is the sum of the forward (k_f) and backward (k_b) reaction rate constants, the two rate constants of $k_f = 0.74 \times 10^{-1} \text{ min}^{-1}$ and $k_b = 1.3 \times 10^{-1} \text{ min}^{-1}$ were obtained. Because k_b is composed of both thermal (k_t) and photoisomerization rate constants, the accelerating backward *cis*-to-*trans* reaction was mainly found to be dominated by the n - π^* absorption of the *cis* isomer in the blue-light region. The calculated *cis* content at the PSS (approximately

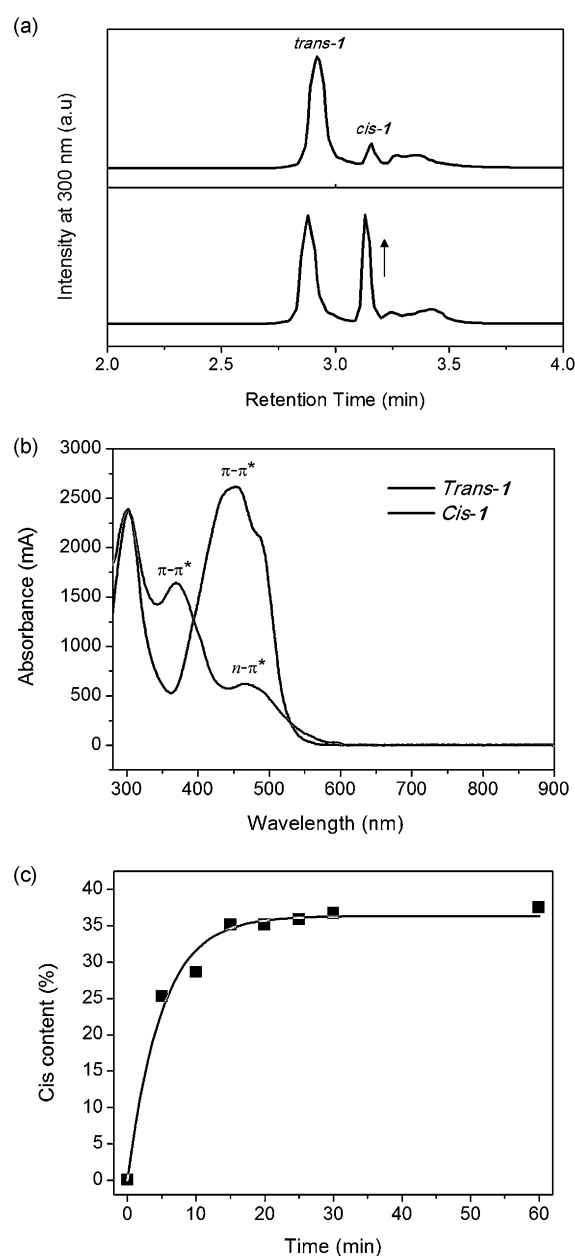


Figure 3. a) HPLC chromatograms for azo compound **1**. The *cis* content gradually increases with blue-light irradiation. b) UV-visible absorption profiles for pure *trans* and *cis* **1** analyzed by HPLC equipped with an on-line photodiode array (PDA) detector. c) Time course of *trans*-to-*cis* photoisomerization. The *cis* content is determined by ^1H NMR spectroscopy, and the solid line is the nonlinear curve fitting integrated rate law. The calculated *cis* content at photostationary state (approximately 36%) is consistent with the experimental value (approximately 35%) obtained using HPLC analysis.

36%), determined from its fit with the nonlinear curve of the rate law, was consistent with the experimental values (approximately 35%) obtained using HPLC analysis.

Because of the efficient nonradiative relaxation process that involves *trans/cis* isomerization, the azo compound **1** was nonfluorescent. Therefore, we introduced an open-aperture fs *Z*-scan technique to examine its 2PA behavior.^[13] Femtosecond laser pulses were generated by a mode-locked

Ti:sapphire laser with a near-infrared (NIR) wavelength of 800 nm, a pulse width of 150 fs, and a repetition rate of 82 MHz. Both the *trans*- and *cis*-**1** were completely transparent at 700–900 nm (Figure 3b), thus suggesting an absence of linear optical absorption in the NIR region. During data collection, laser pulses with a beam waist of approximately 20 μm were focused onto the azo solution in a quartz cuvette with a path length of 1 cm. The incident and transmitted laser powers were monitored as the cuvette moved along the *Z* direction, toward and away from the focus position. Figure 4a shows the experimental *Z*-scan curves of *trans* **1**, which were created by changing the input intensity per laser pulse (I_0), with significant 2PA signatures based on

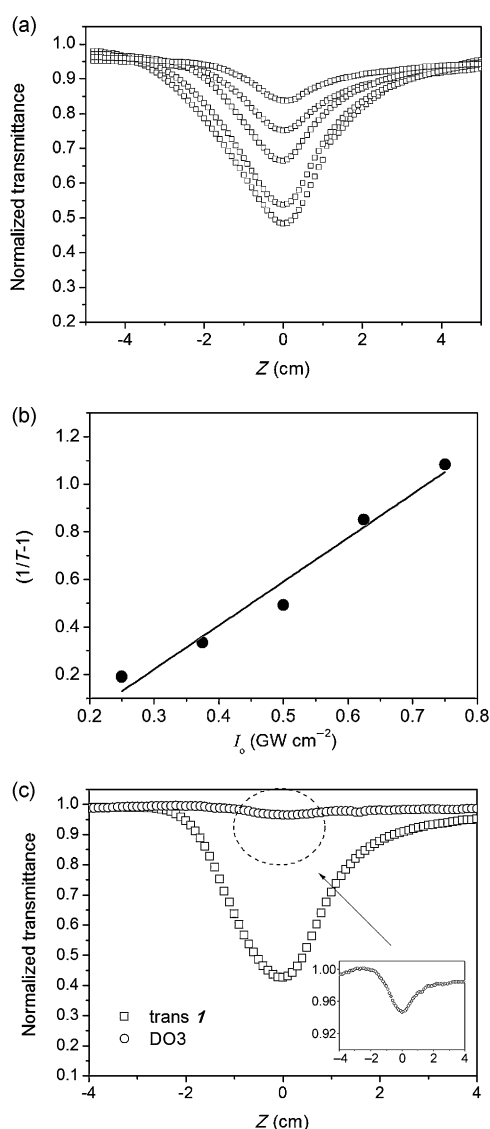


Figure 4. a) Open-aperture *Z*-scan traces of azo compound **1** (5×10^{-3} M in toluene) by changing the input intensity of the laser beam (40, 60, 80, 100, 120 mW) at $\lambda_{\text{ex}}=800$ nm. b) The correlation of $(1/T-1)$ versus I_0 [GW cm^{-2}]; T and I_0 denote the normalized transmittance value at $Z=0$ cm and incident energy per laser pulse, respectively. c) The contrast of the *Z*-scan curves between **1** (1×10^{-2} M in toluene) and DO3 (1×10^{-2} M in THF) under identical input laser intensity (120 mW).

the decrease in normalized transmittance (T) at $Z=0$. The linear dependence between the amplitude of transmittance change $(1/T-1)$ and I_0 also confirms a nonlinear 2PA process (Figure 4b).^[14] Moreover, Figure 4c shows the contrast of *Z*-scan traces between *trans* **1** and Disperse Orange III (DO3), a commercially available NLO azobenzene chromophore (D- π -A type).^[8a,c] Based on the minor change in the transmittance for DO3 under identical I_0 , the 2PA response for *trans* **1** is considerably higher than that for common azo dyes.

Considering the equivocal statement that 2PA intensity is usually lower for azobenzene (Ph-N=N-Ph) than for stilbene (Ph-C=C-Ph) derivatives, combining azo and rigid fluorene with bilateral electron-donating groups did enhance the 2PA cross-section in the NIR wavelength.^[8a] Although there was no clear understanding at the time of this study about the connection between the remarkable 2PA response and azo linkage, our results showed that such a structural combination leads to highly active 2PA chromophores. Furthermore, as shown in Figure 5a, the computational modeling of the

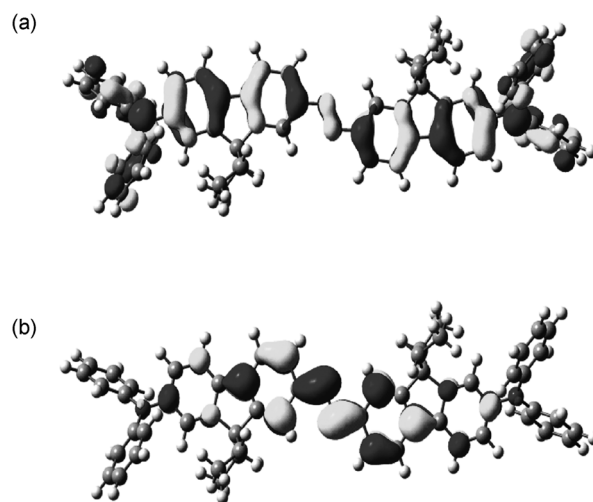


Figure 5. Optimized isosurface plots of the a) HOMO and b) LUMO for *trans*-**1** analogue with 9,9-diethyl substitution, energetically minimized at the density functional B3LYP/6-31G** level under vacuum.

trans-**1** analogue with 9,9-diethyl substitution by using the B3LYP hybrid functional and the 6-31G** basis set shows that the highest-occupied molecular orbital (HOMO) is mainly delocalized over the DPAFs. Meanwhile, the electronic cloud of the lowest-unoccupied molecular orbital (LUMO) is condensed mostly on the central moiety (Figure 5b). This preliminary calculation implies an ICT process from the peripheral diphenylamines (donor) to the central CNNC group (acceptor) through a fluorene π bridge. Moreover, we conjectured that the ICT for azo compound **1** is more favored because of the relatively higher electronegativity of the central nitrogen atoms.

We also analyzed the 2PA intensity of the isomeric mixture at PSS, which was established by blue-light irradiation (approximately 65% of *trans* and 35% of *cis* products).

Prior to the *Z*-scan experiment, the azo solution was exposed to blue light until the PSS was reached, and was then excited in situ by using laser pulses to trace the transmittance change at the focal point. Nevertheless, the normalized change in transmittance at $Z=0$ for the isomeric mixture was nearly identical to that of the all-*trans*-**1** solution (see the Supporting Information). This result implied that, for both solutions, the chemical composition at the laser focusing spot was in the all-*trans* state. This is presumably due to the extremely unstable *cis* structure during the *Z*-scan measurement. The rate constants of k_t for thermal *cis*-to-*trans* back-isomerization substantially increased as the surrounding temperature increased (see the Supporting Information), which suggests that the *cis* isomer became quite unstable with elevating temperatures. Because significant topical heating by laser pulses in high repetition frequency could have induced rapid and complete *cis*-to-*trans* thermal isomerization, the influence on 2PA properties in the presence of the *cis* isomer could not be determined under experimental conditions. Consequently, the preliminary results suggested that the fs 2PA behavior for azo chromophore **1** is quite uniform, regardless of the molecular geometry. To minimize the laser-induced thermal effect, a 2PA experiment that adopted an fs pulse laser with low repetition rate of 1 kHz as an excitation source is now under investigation.

In summary, we successfully demonstrated efficient *trans/cis* photoisomerization and a significant third-order NLO response for the azo chromophore, simply incorporated with bilateral DPAF as a π framework. Although strong electron-donating DPAF moieties could destabilize the central N=N bond, reversibly switching the molecular geometry was still possible through non-coherent LED-light excitation at two wavelengths (466 and 365 nm). The PSS established by using blue light at room temperature was composed of only 36% *cis* isomer. This percentage was mainly due to an increasing *cis*-to-*trans* back-isomerization rate through both photo- ($n-\pi^*$ absorption of *cis* isomer) and thermal isomerization routes. Compared with common azobenzene dyes, the fs *Z*-scan measurement determined a significant enhancement of the 2PA intensity for this azo chromophore in its all-*trans* state. Because of extremely fast *cis*-to-*trans* thermal isomerization under accumulated and substantial heat generated by fs laser pulses, the influence on 2PA properties in the presence of the *cis* isomer was negligible at this stage. Based on different π -conjugation domains, we suggest that the *trans* and *cis* isomers exhibit distinct 2PA behaviors. A thermally stable *cis*-azo chromophore is necessary to achieve a tunable NLO response with respect to a change in molecular geometry.^[11] A study along this line is currently underway, and the findings will be reported in due course.

Experimental Section

Synthesis of Azo Compound **1**

A mixture that contained CuBr (4.6 mg, 32.1 μ mol), pyridine (10 μ L, 0.124 mmol), and 2-amino-substituted diphenylaminofluorene (DPAF,

101 mg, 0.196 mmol) in toluene (2 mL) was purged with air for 5 min, and then stirred vigorously at 60 °C under air balloon for 20 h. After cooling to room temperature and being concentrated under vacuum, the residue was purified by silica flash column chromatography using a *n*-hexane and ethyl acetate mixture (19:1) as eluent to afford an orange solid of **1** (83.8 mg, 83%). ¹H NMR (CDCl₃, 400 MHz): δ = 7.95 (dd, J = 8.1, 1.7 Hz, 2H), 7.90 (d, J = 1.7 Hz, 2H), 7.73 (d, J = 8.1 Hz, 2H), 7.61 (d, J = 8.1 Hz, 2H), 7.29–7.25 (m, 10H), 7.14 (d, J = 8.7 Hz, 8H), 7.03 (t, J = 7.3 Hz, 6H), 2.05–1.96 (m, 4H), 1.92–1.85 (m, 4H), 1.18–1.00 (m, 24H), 0.79 (t, J = 7.1 Hz, 12H), 0.69 ppm (m, 8H); ¹³C NMR (CDCl₃, 100 MHz): δ = 153.5, 152.1, 151.9, 148.1, 144.0, 135.5, 129.5, 124.3, 123.5, 123.1, 123.0, 121.3, 119.6, 119.1, 117.1, 55.5, 40.6, 31.8, 30.0, 24.1, 22.8, 14.3 ppm; MALDI-TOF-MS: m/z calcd for C₇₄H₈₅N₄ [M+H]⁺: 1029.68; found: 1029.81.

Acknowledgements

The authors would like to thank the Ministry of Science and Technology of Taiwan (MOST102-2113M-040-004) for financially supporting this research. The authors are also grateful to Prof. Toyoko Imae for support with micro-Raman measurements and to Prof. Ming-Yu Kuo for support with the computational modeling.

Keywords: absorption • azo compounds • charge transfer • chromophores • isomerization

- [1] a) Y. Zhao, T. Ikeda in *Smart Light-Responsive Materials: Azobenzene-Containing Polymers and Liquid Crystals*, Wiley, New Jersey, **2009**; b) R. Deloncle, A.-M. Caminade, *J. Photochem. Photobiol. C* **2010**, *11*, 25–45; c) M. Han, T. Honda, D. Ishokawa, E. Ito, M. Hara, Y. Norikane, *J. Mater. Chem.* **2011**, *21*, 4696–4702; d) S. Samanta, A. A. Beharry, O. Sadowski, T. M. McCormick, A. Babalhavaji, V. Tropepe, G. A. Woolley, *J. Am. Chem. Soc.* **2013**, *135*, 9777–9784; e) S.-L. Chen, C.-C. Chu, V. K. S. Hsiao, *J. Mater. Chem. C* **2013**, *1*, 3529–3531.
- [2] N. Tamai, H. Miyasaka, *Chem. Rev.* **2000**, *100*, 1875–1890.
- [3] a) Y. Norikane, N. Tamaoki, *Org. Lett.* **2004**, *6*, 2595–2598; b) K. G. Yager, C. J. Barrett, *J. Photochem. Photobiol. A* **2006**, *182*, 250–261; c) D. P. Ferris, Y.-L. Zhao, N. M. Khashab, H. A. Khatib, J. F. Stoddart, J. I. Zink, *J. Am. Chem. Soc.* **2009**, *131*, 1686–1688; d) S. K. M. Nalluri, J. Voskuhl, J. B. Bultema, E. J. Boekema, B. J. Ravoo, *Angew. Chem. Int. Ed.* **2011**, *50*, 9747–9751; *Angew. Chem.* **2011**, *123*, 9921–9925; e) I. Tochitsky, A. Polosukhina, V. E. Degtyar, N. Gallerani, C. M. Smith, A. Friedman, R. N. Van Gelder, D. Trauner, D. Kaufer, R. H. Kramer, *Neuron* **2014**, *81*, 800–813.
- [4] J. A. Delaire, K. Nakatani, *Chem. Rev.* **2000**, *100*, 1817–1845.
- [5] Z. Sekkat, P. Prêtre, A. Knoesen, W. Volksen, V. Y. Lee, R. D. Miller, J. Wood, W. Knoll, *J. Opt. Soc. Am. B* **1998**, *15*, 401–413.
- [6] a) G. S. He, L.-S. Tang, Q. Zheng, P. N. Prasad, *Chem. Rev.* **2008**, *108*, 1245–1330; b) R. Rumi, S. Barlow, J. Wang, J. W. Perry, S. R. Marder, *Adv. Polym. Sci.* **2008**, *213*, 1–95; c) H. Xia, W.-Y. Zhang, F.-F. Wang, D. Wu, X.-W. Liu, L. Chen, Q.-D. Chen, Y.-G. Ma, H.-B. Sun, *Appl. Phys. Lett.* **2009**, *95*, 083118; d) S. Yao, K. D. Belfield, *Eur. J. Org. Chem.* **2012**, 3199–3217; e) H. Wang, F. Jin, S. Chen, X.-Z. Dong, Y.-L. Zhang, W.-Q. Chen, Z.-S. Zhao, X.-M. Duan, *J. Appl. Polym. Sci.* **2013**, *130*, 2947–2956.
- [7] a) M. Albota, D. Beljonne, J. L. Brédas, J. E. Ehrlich, J.-Y. Fu, A. A. Heikal, S. E. Hess, T. Kogej, M. D. Levin, S. R. Marder, D. McCord-Maughon, J. W. Perry, H. Röckel, M. Rumi, G. Subramaniam, W. W. Webb, X.-L. Wu, C. Xu, *Science* **1998**, *281*, 1653–1656; b) K. D. Belfield, Y. Liu, R. A. Negres, M. Fan, G. Pan, D. J. Hagan, F. E. Hernandez, *Chem. Mater.* **2002**, *14*, 3663–3667; c) S. Yao, H.-Y. Ahn, X. Wang, J. Fu, E. W. V. Stryland, D. J. Hagan, K. D. Belfield, *J. Org. Chem.* **2010**, *75*, 3965–3974; d) T.-C. Lin, M.-H. Li, C.-Y. Liu, J.-H.

- Lin, Y.-K. Shen, Y.-H. Lee, *J. Mater. Chem. C* **2013**, *1*, 2764–2772; e) T.-C. Lin, C.-Y. Liu, B.-R. Huang, J.-H. Lin, Y.-K. Shen, C.-Y. Wu, *Eur. J. Org. Chem.* **2013**, 498–508.
- [8] a) L. Antonov, K. Kamada, K. Ohta, F. S. Kamounah, *Phys. Chem. Chem. Phys.* **2003**, *5*, 1193–1197; b) S. W. Magennis, F. S. Mackay, A. C. Jones, K. M. Tait, P. J. Sadler, *Chem. Mater.* **2005**, *17*, 2059–2062; c) L. De Boni, L. Misoguti, S. C. Zilio, C. R. Mendonca, *ChemPhysChem* **2005**, *6*, 1121–1125; d) T. V. Truong, C.-Y. Chen, N. V. Tabiryan, Y. R. Shen, *J. Opt. Soc. Am. B* **2007**, *24*, 2623–2626; e) L. D. Boni, A. A. Andrade, S. B. Yamaki, L. Misoguti, S. C. Zilio, T. D. Z. Atvars, C. R. Mendonca, *Chem. Phys. Lett.* **2008**, *463*, 360–363.
- [9] C. Zhang, N. Jiao, *Angew. Chem. Int. Ed.* **2010**, *49*, 6174–6177; *Angew. Chem.* **2010**, *122*, 6310–6313.
- [10] a) C.-M. Stuart, R. R. Frontiera, R. A. Mathies, *J. Phys. Chem. A* **2007**, *111*, 12072–12080; b) Y. B. Zheng, J. L. Payton, C.-H. Chung, R. Liu, S. Cheunkar, B. K. Pathem, Y. Yang, L. Jensen, P. S. Weiss, *Nano Lett.* **2011**, *11*, 3447–3452.
- [11] B.-K. Tsai, C.-H. Chen, C.-H. Hung, V. K. S. Hsiao, C.-C. Chu, *J. Mater. Chem.* **2012**, *22*, 20874–20877.
- [12] L. Li, F. He, X. Wang, N. Ma, L. Li, *ACS Appl. Mater. Interfaces* **2012**, *4*, 4927–4933.
- [13] a) J.-H. Lin, Y.-J. Chen, H.-Y. Lin, W.-F. Hsieh, *J. Appl. Phys.* **2005**, *97*, 033526; b) Y.-P. Chan, J.-H. Lin, C.-C. Hsu, W.-F. Hsieh, *Opt. Express* **2008**, *16*, 19900–19908; c) M. Wang, V. Nalla, S. Jeon, V. Mamidala, W. Ji, L.-S. Tan, T. Cooper, L. Y. Chiang, *J. Phys. Chem. C* **2011**, *115*, 18552–18559.
- [14] a) A. A. Said, M. Sheik-Bahae, D. J. Hagan, T. H. Wei, J. Wang, J. Young, E. W. V. Stryland, *J. Opt. Soc. Am. B* **1992**, *9*, 405–414; b) W. J. Yang, D. Y. Kim, C. H. Kim, M.-Y. Jeong, S. K. Lee, S.-J. Jeon, B. R. Cho, *Org. Lett.* **2004**, *6*, 1389–1392; c) K. D. Belfield, M. V. Bondar, F. E. Hernandez, O. V. Przhonska, S. Yao, *J. Phys. Chem. B* **2007**, *111*, 12723–12729.


Received: July 29, 2014
Published online: ■ ■ ■, 0000

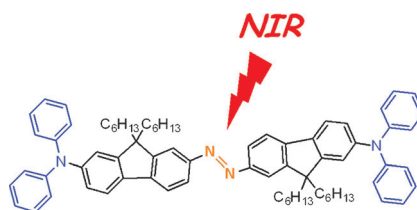
COMMUNICATION

Photoisomerization

Chih-Chien Chu,* Ya-Chi Chang,
Bo-Kai Tsai, Tzu-Chau Lin,
Ja-Hon Lin,
Vincent K. S. Hsiao



 ***trans/cis*-Isomerization of Fluorene-Bridged Azo Chromophore with Significant Two-Photon Absorbability at Near-Infrared Wavelength**



Light absorber: A fluorene-bridged azo chromophore shows an intense π - π^* absorption in the blue-light region, thus allowing a *trans*-to-*cis* photoisomerization under blue light-emitting diode (LED) excitation (see scheme). The azo material also has significant two-photon absorption in the near-IR wavelength under the excitation of a femtosecond pulse laser beam.

科技部補助計畫衍生研發成果推廣資料表

日期:2015/01/03

科技部補助計畫	計畫名稱: 開發以破六十為核心之兩性自組裝樹枝狀高分子在基因載體上的研究
	計畫主持人: 朱智謙
	計畫編號: 102-2113-M-040-004- 學門領域: 有機化學
無研發成果推廣資料	

102 年度專題研究計畫研究成果彙整表

計畫主持人：朱智謙		計畫編號：102-2113-M-040-004-					
計畫名稱：開發以碳六十為核心之兩性自組裝樹枝狀高分子在基因載體上的研究							
成果項目		量化			單位	備註（質化說明：如數個計畫共同成果、成果列為該期刊之封面故事...等）	
		實際已達成數（被接受或已發表）	預期總達成數（含實際已達成數）	本計畫實際貢獻百分比			
國內	論文著作	期刊論文	0	0	100%	篇	
		研究報告/技術報告	0	0	100%		
		研討會論文	4	5	80%		
		專書	0	0	100%		
	專利	申請中件數	0	0	100%	件	
		已獲得件數	0	0	100%		
	技術移轉	件數	0	0	100%	件	
		權利金	0	0	100%	千元	
	參與計畫人力 （本國籍）	碩士生	2	2	100%	人次	
		博士生	0	0	100%		
博士後研究員		0	0	100%			
專任助理		0	0	100%			
國外	論文著作	期刊論文	3	4	75%	篇	
		研究報告/技術報告	0	0	100%		
		研討會論文	0	0	100%		
		專書	0	0	100%		章/本
	專利	申請中件數	0	0	100%	件	
		已獲得件數	0	0	100%		
	技術移轉	件數	0	0	100%	件	
		權利金	0	0	100%	千元	
	參與計畫人力 （外國籍）	碩士生	0	0	100%	人次	
		博士生	0	0	100%		
博士後研究員		0	0	100%			
專任助理		0	0	100%			

<p style="text-align: center;">其他成果</p> <p>(無法以量化表達之成果如辦理學術活動、獲得獎項、重要國際合作、研究成果國際影響力及其他協助產業技術發展之具體效益事項等，請以文字敘述填列。)</p>	<p>無。</p>
---	-----------

	成果項目	量化	名稱或內容性質簡述
科 教 處 計 畫 加 填 項 目	測驗工具(含質性與量性)	0	
	課程/模組	0	
	電腦及網路系統或工具	0	
	教材	0	
	舉辦之活動/競賽	0	
	研討會/工作坊	0	
	電子報、網站	0	
	計畫成果推廣之參與(閱聽)人數	0	

科技部補助專題研究計畫成果報告自評表

請就研究內容與原計畫相符程度、達成預期目標情況、研究成果之學術或應用價值（簡要敘述成果所代表之意義、價值、影響或進一步發展之可能性）、是否適合在學術期刊發表或申請專利、主要發現或其他有關價值等，作一綜合評估。

1. 請就研究內容與原計畫相符程度、達成預期目標情況作一綜合評估

達成目標

未達成目標（請說明，以 100 字為限）

實驗失敗

因故實驗中斷

其他原因

說明：

2. 研究成果在學術期刊發表或申請專利等情形：

論文： 已發表 未發表之文稿 撰寫中 無

專利： 已獲得 申請中 無

技轉： 已技轉 洽談中 無

其他：（以 100 字為限）

3. 請依學術成就、技術創新、社會影響等方面，評估研究成果之學術或應用價值（簡要敘述成果所代表之意義、價值、影響或進一步發展之可能性）（以 500 字為限）

本計劃目標為兩親性樹枝狀分子的合成製備、DNA 複合體的型態分析與物理化學性質分析、以及初步基因轉染效率的探討。自評目前的研究成果符合原先設定之目標。我們利用高效率的合成方法合成出一系列兩性基因載體，經過初步測試後證明此材料具有不錯的 DNA 結合能力與光控釋放能力。目前正在積極嘗試 *in vivo* 細胞生物相關研究。基於這些發現，除了能夠發表相關的學術論文之外，也可以思考申請專利與產學合作的可能性。